IMPROVING THE ACCUMULATION OF GOLD NANOPARTICLES USING ULTRASOUND AND MICROBUBBLES TO ENHANCE RADIATION THERAPY

by

Mathew John Rajic

H.B.Sc University of Toronto, 2015

Toronto, Canada

A thesis

presented to Ryerson University

in partial fulfillment of the

requirements for the degree of

Master of Science

in the program of

Biomedical Physics

Toronto, Ontario, Canada, 2019

AUTHOR'S DECLARATION

I hereby declare that I am the sole author of this thesis. This is a true copy of the thesis, including any required final revisions, as accepted by my examiners.

I authorize Ryerson University to lend this thesis to other institutions or individuals for the purpose of scholarly research

I further authorize Ryerson University to reproduce this thesis by photocopying or by other means, in total or in part, at the request of other institutions or individuals for the purpose of scholarly research.

I understand that my thesis may be made electronically available to the public.

Mathew Rajic

Abstract

IMPROVING THE ACCUMULATION OF GOLD NANOPARTICLES USING ULTRASOUD AND MICORBUBBLES TO ENHANCE RADIATION THERAPY

Mathew John Rajic

Master of Science, Biomedical Physics

Ryerson University, 2019

Gold nanoparticles have long been considered for use in conjunction with radiation therapy to enhance dose in a local tumor regions. However, limitation in cellular accumulation remains a hindrance for treatments to extend to clinical levels. Ultrasound and microbubbles have been shown to enhance the delivery of chemotherapies, genetic material and other molecules. This goal of this study was to demonstrate, for the first time to the best of our knowledge, the increase in PEGylated gold nanoparticle accumulation in cells due to the addition of ultrasound and microbubbles, and survival fraction. The results display approximate 3 fold increase in intracellular gold content independent of nanoparticle size, resulting in a 5 fold increase in cell death. Additionally, it was shown that USMB can facilitate nuclear localization of gold nanoparticles with nuclear localized signals to further enhance radiation therapy.

Acknowledgements

I would like to think first and foremost my patient supervisor Dr. Raffi Karshafian, without whom I would not have had this wonderful experience to learn and grow. I know I can be difficult to work with and your guidance and support came without complaint. Words just aren't enough to thank you properly.

I would also like to thank my supervisory committee Dr. Ana Pejović-Milić, and Dr. Costin Antonescu who helped me through my degree. Without your helpful guidance, and great patience, I would still be at square one.

I must also thank my fellow lab mates, Aren Gharabeiki, Charlotte Ferworn, Victoria Bulycheva and Rahul Misra who made my tough days bearable, my good days better, and my great days amazing. I would especially like to thank Aren for his help in my experiments, letting me in the lab at 6:00 a.m. when I forgot my badge, and mostly sharing in my failures, without you I would have lost my mind more than I have. I would also like to thank Rhea Salinas for her help with preparing microscope slides when 24 hours and one pair of hands just weren't enough.

Lastly, I would like to thank my family, who may not know what my degree is called, but love me for it anyway.

Dedication

To my loving mom, without whom I would not be here today

Table of Contents

Symbols and Abbreviations

AuNP- gold nanoaprticles

DNA- deoxyribose nucleuic acid

EPR- enhanced permeability and retention

FFT- Fast Fourier Transform

ICD- integrated cavitation dose

ICP AES- Inductively coupled plasmon atomic emission spectroscopy

NLS- nuclear localizing signal

SPR- surface plasmon resonance

USMB- ultrasound and microbubbles

V_c- clonogenic viability in survivial fraction

V_a- additive survival fraction calculated using Bliss criteria

XRT- x-ray radiation therapy

List of figures

Chapter 1 Introduction

1.1 Background and Motivation

Limitations of X-ray Radiation Therapy (XRT), such as safe dose limitations and the inability of ionizing radiation to distinguish between tumor tissue and healthy tissue have led the field to find methods to enhance the effectiveness of radiation damage. Gold Nanoparticles, due to their high atomic number and biocompatibility have emerged as desirable method to achieve this radiation enhancement. By injecting gold nanoparticles into the vasculature or directly into the tumor region, it has been shown both in vivo [1,2] and in vitro [3–6], that gold nanoparticles can enhance the efficacy of radiation treatments.

The use of gold nanoparticles has been unsuccessful in establishing itself in clinical practices, largely in part to its poor delivery into tumor regions and cancer cells. An intensive review of nanoparticle delivery has shown that the average accumulation of gold nanoparticles within the tumor (under varying conditions) is 1% of the administered mass[6]. While the premise of radiation enhancement by heavy atoms like gold is largely explored in vivo and in vitro, the poor accumulation remains a large obstacle for feasible treatment options[6 7]. The main motivation of this research is to improve upon the cellular delivery of gold nanoparticles, by the use of ultrasound and microbubbles (USMB).

Developed initially as ultrasound contrast agents, microbubbles have been shown to enhance the cellular delivery of fluorescent molecules[8], chemotherapies[10–15], as well as provide a method of gene transfection[9,13–16], by transient permeabilizing of the cellular membrane [17–23], a process broadly referred to as sonoporation. Microbubble oscillations caused by exposure to an ultrasound field can reversibly generate pores on cell membranes, allowing for passive diffusion of molecules from the extracellular matrix to the cytoplasm[18,19,22] . Additionally, cells exposed to ultrasound and microbubbles have demonstrated increased rates of endocytosis[17,24,25] as well as increased rates of pinocytosis[26] .

While ultrasound and microbubbles have been used in combination with chemotherapy to improve treatment efficacy in vitro, in vivo and most notably in clinical trials[11], little work has been done

combining the treatment with radiation and less still in combination with radioenhancers, specifically gold nanoparticles. This research attempts to progress the gold nanoparticle field by overcoming the natural limits of cellular uptake with the assistance of ultrasound and microbubbles. Prostate cancer is an ideal model for this study, as current treatments include radiation therapy. Brachytherapy is a common radiation treatment option which benefits more from the enhancement AuNP can provide because the lower energy treatment is favorable for the photoelectric effect. Additionally, insertion of the catheters for brachytherapy seeds is guided by ultrasound systems, which can be used in conjunction with microbubbles.

1.2 Radiotherapy

The international Agency of research of cancer estimates that 7.6 million deaths and over 12 million cases arise worldwide yearly[27]. Discoveries over a century ago, x-rays have had a clinical application developing the field of radiation therapy. Now radiation therapy is used in 50% of all cancer cases, and it is incorporated in 40% of all curative treatments[27].

Radiation therapy attempts to provide a lethal dose of Ionizing radiation mainly in the form of external x-ray beams, typically generated from the 6-18 MV range, to affected tissues. Typically relying on Compton scattering interactions, means there is a lack of target specificity as Compton scattering crossection is independent of target characteristics like atomic number, additionally contrast between tumor and healthy tissue is poor[28]. Thus treatments are limited by the ability to reduce dose to surrounding tissues. Developments of different forms of radiation therapy such as brachytherapy, proton therapy, as well as new techniques like Intensity- modulated radiotherapy, attempt to deliver radiation dose in different methods to focus on affected tissues while sparing surrounding healthy tissues.

1.3 Radiation Sensitizers

Improvements to radiotherapy typically aim to reduce dose to healthy tissue in the proximity to target regions. Techniques like intensity modulation improve the ability to deliver Ionizing radiation in a focused and more precise manor, sparing unaffected healthy tissue the full dose of radiation. Alternatively, other avenues of research attempt to increase the effectiveness of radiation therapy itself. Molecules that promote direct and indirect damage to DNA such as some chemotherapeutics like gemcitabine, reduce the cells ability to repair damage, or those that increase the local dose delivered during radiotherapy can increase the overall effectiveness of radiotherapy. Molecules that increase the efficacy of radiation therapy in this way are referred to as radiosensitizers, and by improving the damage to cancer cells in a local region, the overall dose delivered can be reduced, sparing unwanted effects from the surrounding tissues or the damage done by radiation can be increased without increasing the risk to the patients[29].

Gold nanoparticles have been found to be a radiosensitizer that increases the actual dose delivered within a local region, by absorbing comparatively more Ionizing x-rays than tissues[30]. Gold's high atomic number of 79 increases the probability of photoelectric interactions between high energy photons and the gold molecule. These interactions cause more energy to be absorbed as the ionizing radiation passes through the tissue, which is causes the release of electrons from the gold atoms. These electrons can directly damage DNA, or can indirectly cause damage by generating free radicals.

The phenomenon occurring when high Z materials interact with Ionizing radiation was first realized when Iodine was used as a contrast agent for imaging. The higher atomic number of Iodine relative to common elements in tissues increases the contrast in X-ray images by absorbing more photons than regular tissue. Due to the nature of Ionizing radiation, the increased absorption causes ionization by a release of electrons which can then interact with the tissue. This increased the effective dose in a local region near the Iodine, which was circulating in the blood. Thus, the effect was observed in circulating lymphocytes where an increased rate of chromosomal deformations was observed[31]. Following this discovery Iodine was used to increase the efficacy of radiation therapy in mice and in vitro in the form of IUdr significant effect[32]. Problematically the amount of Iodine required to generate a significant radio enhancement effect has toxic side effects to patients, and the use of Iodine has been overshadowed by the use of more biocompatible and optimal radioenhancers.

1.4 AuNP

Gold nanoparticles, typically ranging from 2-100 nm in diameter have become more popular than iodine as a radiosensitizer due to its larger Z and biocompatibility [33]. The significantly greater Z allows for triple the photoelectric crossection in the presence of relevant energies of ionizing radiation[34].

The first major attempt to demonstrate the potential for radiation enhancement by AuNP was done by Hainfeld et al, in 2004. The injected mice with 2.7mg/g of gold compared to their body weight yielding about 0.7% gold by mass inside the tumor. The 1 year survival was increased to 86% vs 20%[1]. The large amount of AuNP added displayed the biocompatibility, and the excellent results inspired the

field to seriously consider gold nanoparticles as a useful radiosensitizer. In this study, direct injections of the nanoparticles were also explored but ultimately yielded worse results due to irregular distribution of the nanoparticles. The main limitations of this study, as stated by the author, was the excess amount of AuNP used, addressing that for clinical feasibility, a method to reduce the required gold would be necessary[1].

1.4.1 Mechanism; Size and Location Dependence

The radiation enhancement observed when heavy metal particles are present in close proximity to affected cells is due to the nature of the photoelectric effect. The photoelectric effect crossection is dependent upon the ratio of $\frac{Z^3}{E}$, where Z is the atomic number and E is the incident photon energy. As the atomic number increases, the probability of photoelectric interactions increase greatly especially at lower levels of ionization energy.

Incident photons that have enough energy to eject an inner shell electron, called the photoelectron, will leave vacancies in the electron shell of the atom. Those vacancies are filled with higher energy electrons in further orbits, as they release the difference in energy between the vacancy shell and their current energy. The energy released takes the form of a characteristic x-ray with a predictable wavelength dependent on the difference in energy between the vacancy shell and the shell the higher energy electron dropped from. Alternatively, the excess energy released can be used to eject another electron in a further shell, called an Auger electron[35]. This additional ejection leaves another vacancy in the atoms electron shell which can be filled by another outer shell electron releasing more excess energy to drop down in energy state. As a result, multiple Auger electrons can be released from a single photoelectric event to fill the shell vacancies generated by the previous emission of Auger electrons. This event is referred to as an Auger cascade [35,36]. These emitted electrons can directly or indirectly cause DNA damage, which is the mechanism that high metal atoms are radiation sensitizations.

Furthermore, due to the nature of the photoelectric effect and Auger Cascade, the effectiveness of gold nanoparticles to increase the radiation dose locally is dependent on size of the nanoparticles. The incident photon can deposit a large amount of energy to the photoelectron, therefore the range of the photoelectron can be tens of micrometers[37,38]. This means that the photoelectron can deposit its energy in a path within 200 nm from the gold nanoparticle. The photoelectron can provide near around 50% of the energy released from the gold nanoparticle during a photoelectric event. At ideal energies for radiation enhancement from gold nanoparticles where photoelectric effects dominate the photon interaction, near 10-80 keV, Auger electrons contribute to near 30% of the energy release by the photoelectric event[38]. The remaining percentage of energy is internally absorbed by the gold nanoparticle and does not contribute to the radio sensitization effect. A Monte Carlo study performed by Pignol et al, calculated the energy release resulting from photoelectric events in different forms (Auger electron, photoelectron, characteristic x-ray and internal absorption) and showed its dependence on nanoparticle size and incident photon energy shown in figure 1-1[39]. The internal absorption is due to the relatively low range of Auger electrons. As the Auger electrons travel through the gold nanoparticles, some of the energy is absorbed by the gold itself. The larger the particle, the greater the path length the electron travels and the greater the amount of energy is absorbed by the gold atoms. Thus from a physical perspective, the smaller the gold nanoparticles, the more potential for radiosensitization assuming the same mass of gold is being considered[38,40].

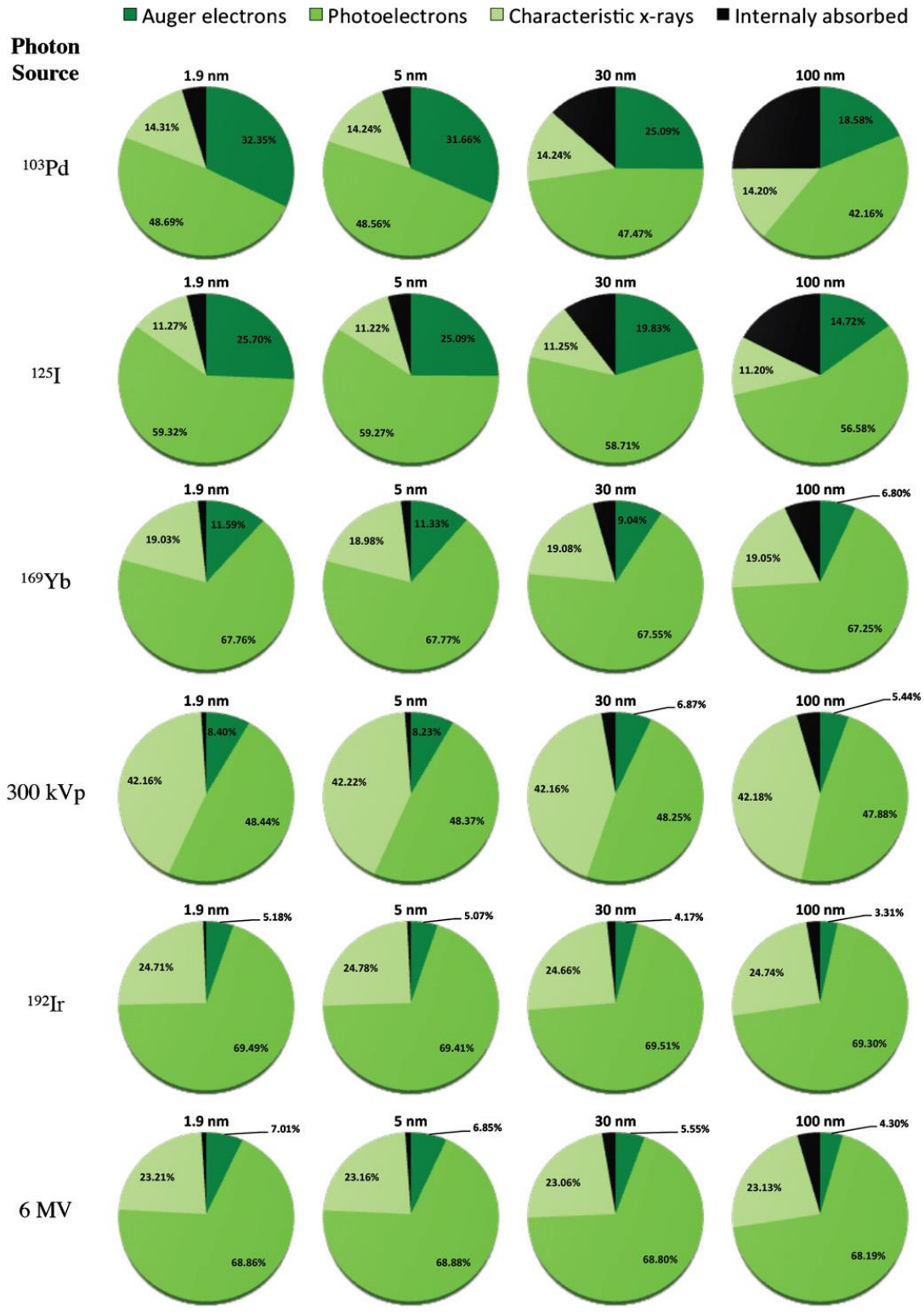

Figure 1-1[39]: Graphical representation of Monte Carlo simulated energy releases for photo electric events. Size increases from left to right while incident photon energy increases top to bottom. As incident energy increases, there is less emitted energy in the form of Auger electrons, but there is also less probability for phot electric incidents to occur. As the particles get larger, it is evident that more of the Auger electron energy becomes internally absorbed.

Also a consequence of the low range of Auger electrons and to a lesser extent photo electrons, is the radiosensitization dependence on gold nanoparticle distance to the target. Because the electrons deposit energy along their path, and in the case of the Auger electrons ejected due to incident photons with optimal energies, all their energy is typically deposited within 200nm of the gold nanoparticles[30,41], close proximity to the radiation target is ideal for maximum effectiveness. In one Monte Carlo Study it is estimated that the nuclear dose increases 2 fold for nanoparticles when they are in the nucleus as opposed to the cytoplasm[30]. Therefore, to maximize the effect of gold nanoparticles, the particle themselves ideally would be internalized in the cancerous cells and localized within the nucleus.

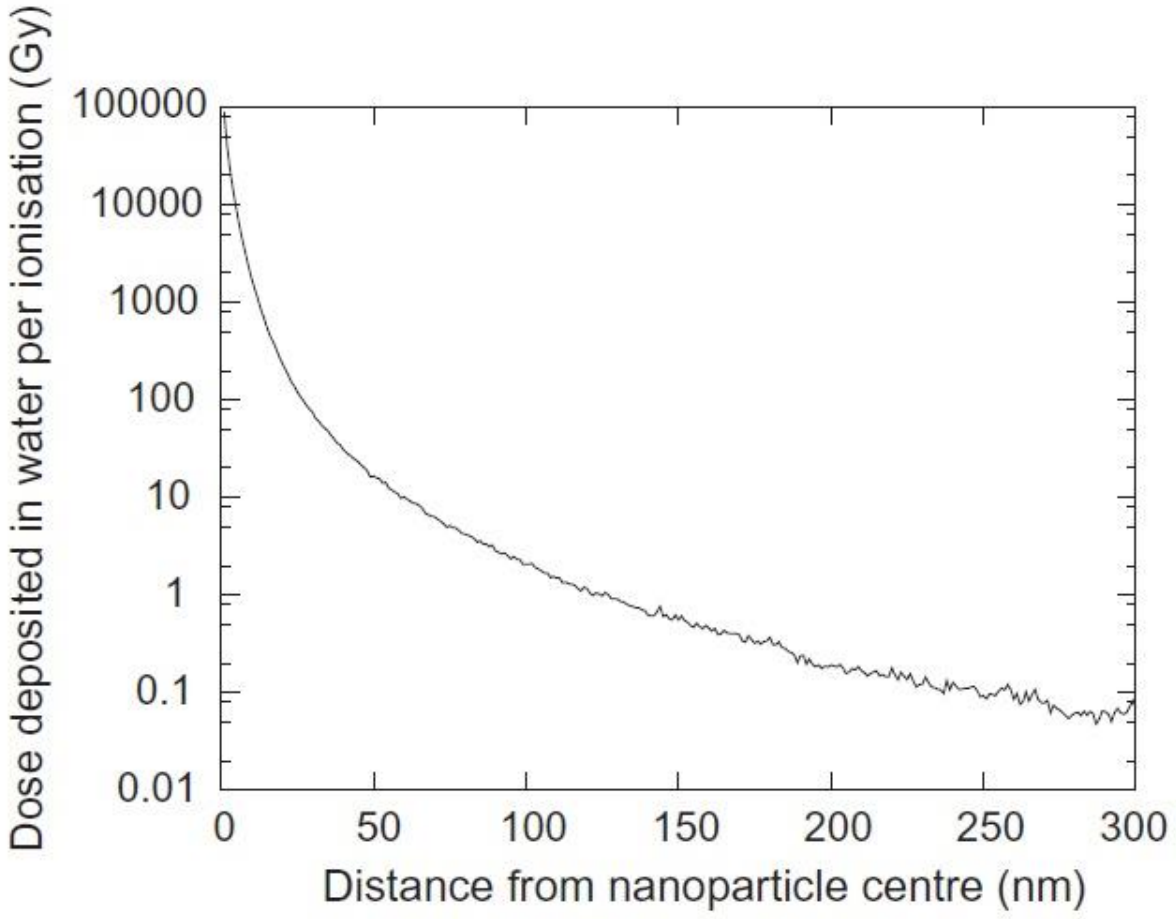

Figure 1-2[38]: Monte Carlo simulated Dose in Gy deposited from the centre of a AuNP measured in nm, at 6 MeV excitation energy. This simulation clearly depicts the extremely local dose distribution achieved from Auger electrons with significant decay past 200 nm, emphasizing the localization requirement for optimal radiosensitization.

1.4.2 AuNP Cellular Uptake

Gold nanoparticle localization within cells is paramount for effective radiosensitization, because dose enhancement declines rapidly with distance from the nanoparticle. As a result, cellular accumulation, has been a focus in the study for gold nanoparticle assisted radiotherapy. Gold nanoparticles typically enter cells through receptor mediated endocytosis[42,43]. Both clathrin and caveolae based endocytosis has been shown to be responsible for at least some of the cellular accumulation[3,44].

Various characteristics of the gold nanoparticles play a role in cellular accumulation. The surface of the nanoparticle, both in charge and chemistry is one of those characteristics. Due to the negative dipole on the phosphate group at end of phospholipids that comprise the cell membrane, it has been found that a positive surface charges are more optimal than either negative or neutral charges for cellular accumulation[3]. While beneficial on a cellular level, charged nanoparticles have been shown to have significantly shorter circulation time in vivo due to macrophage targeting[45], developing a tradeoff between cellular uptake and having enough particles circulating to achieve an adequate amount of nanoparticles in the tumor region. Consequently, it has also been shown that specific coatings on nanoparticles can facilitate specific cell targeting by using the overexpression of surface proteins on cell membranes, or other coatings can facilitate intercellular targeting[46]. Other coatings like CTAB are common for gold nanorods and allows for interactions with the mitochondrial membrane.

To further optimize localization of AuNP within the cellular environment, peptides like a nuclear localizing signal (NLS) can be attached to the nanoparticle surface. This specific surface coating interacts with the Importin alpha and beta proteins found in the cytoplasm of cells. Importin's function is to act as a vehicle, transporting bound molecules to nuclear pores. These nuclear pores can allow molecules with a maximum diameter of 30nm to enter the nucleus[47,48]. As discussed previously, radiation sensitization is dependent on the proximity of the sensitizer and the target. Since DNA is considered the primary target for radiation damage, nuclear localization should improve the local dose enhancement leading to even greater treatment efficacy. However, for this nuclear localization to be possible the NLS signal needs to

interact with Importin in the cytoplasm. The typical uptake pathways for AuNP are different types of nonspecific endocytosis, which leaves the nanoparticles inside endosomes and eventually lysosomes, restricting contact with materials in the cytoplasm. Studies have shown that directly injecting particles with a nuclear localizing signal into the cytoplasm of cells will allow those particles to collect in the nucleus, but when those same particles are exposed to cells and enter through endocytosis, they cannot enter the nucleus[49]. Further studies have determined that adding specific coatings in addition to NLS will allow for the particles to escape the endosomes. Studies have shown that RGD peptides allow for nuclear uptake when in conjunction with NLS as shown in figure 3-1. It is theorized that RGD peptides causes the endosome to disassociate, freeing the particle[49,50].

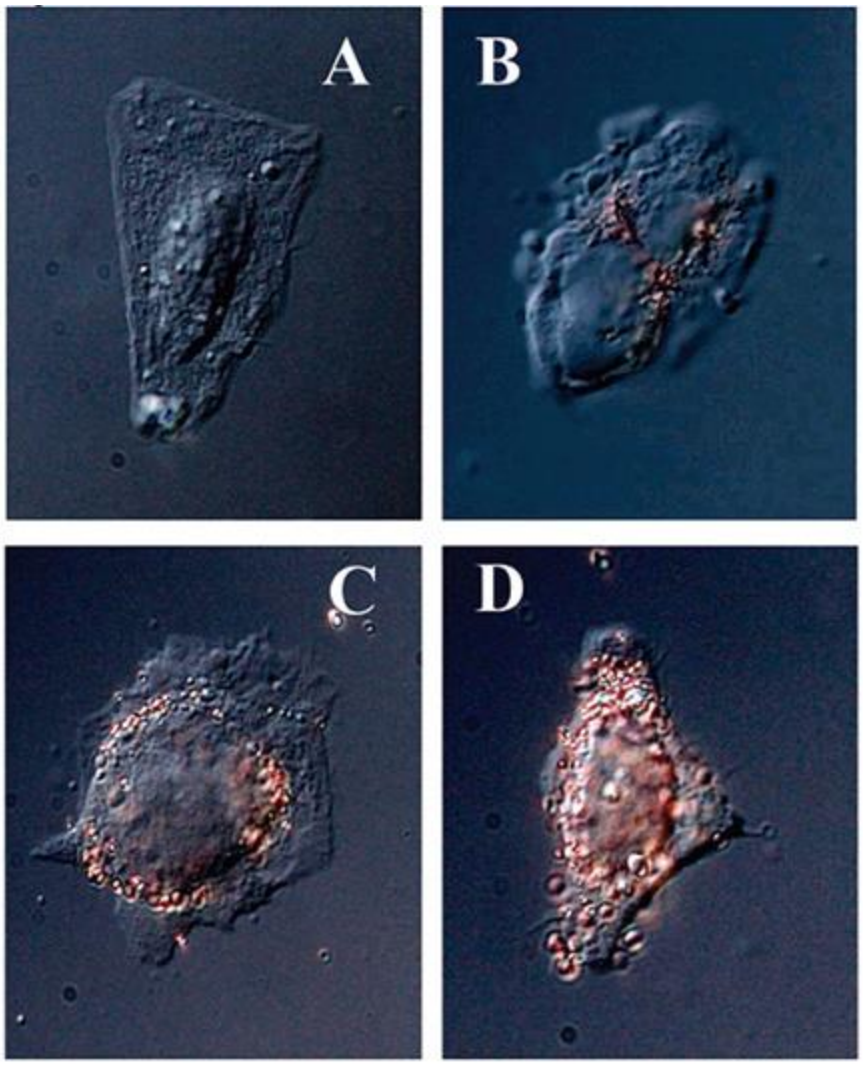

Figure 1-3[49]: Leica DMLB DIC equipped microscope images of A) HEPG2 cells B) Cells incubated with 20 nm AuNP with a NLS signal, C)Cells incubated with 20 nm AuNP with NLS attached to RGD. C) Cells incubated with 20 nm AuNP with NLS alongside RGD. It is evident that NLS was not able to transfer AuNP to the nucleus, but required RGD peptides, the most effective of which was when they were placed alongside each other.

Other important factors that contributes to nanoparticle accumulation is nanoparticle size and shape. While smaller nanoparticles are ideal for radio sensitization, due to lower amounts of energy from Auger electrons being internally absorbed, size dependence on accumulation favours different characteristics. Nanoparticles of about 50 nm have been shown to have the greatest amount of cellular accumulation in vitro[4]. Smaller particles have been shown to have poor retention, often being exocytosed at a faster rate than larger ones[5]. Particles larger than 50 nm also have poor cellular accumulation due to limitations on endosome sizes; larger endosomes are less energy favourable and occur less frequently. In

the field of gold nanoparticles, the greatest consensus is that 50 nm nanoparticles, while less favourable in some respects, are ideal for cellular accumulation. Gold nanoparticles are most commonly designed in two shapes, spheres which we have been discussing thus far, and rods. Rods are used primarily for photo thermal therapy or other optically inclined modalities due to the ideal peak of absorbance. Metal nanoparticles often express very specific absorbance and scattering patterns based on their size and shape, because of a phenomenon called Surface Plasmon Resonance[51]. Gold nanorods in particular have a peak absorbance (dependent on size) within the near infrared region, which is an ideal wavelength to avoid common absorbers in tissue such as oxygenated and deoxygenated blood. The increased absorbance of the nanorods allows for localized heating which can enhance cell death in radiation therapy as well as for use as optical markers for diagnostic purposes[52]. Spherical AuNP have greater accumulation than nanorods and will be used in this study[4].

1.4.3 AuNP Accumulation in Vivo

Nanoparticles can be delivered to tumor tissue intravenously and through direct injection into the tumor tissue. Tumor type and location limit the feasibility of directly injecting the nanomaterial, and studies have shown that often direct injections lead to a non-uniform distribution of the particles only affecting certain regions of the tumor[1]. Thus, the ability for nanoparticles to circulate and diffuse from the blood vessels into affected tissues is vital, and nanoparticle size also factors into this. Past studies have relied on the enhanced permeability and retention (EPR) characteristics of tumors, which is caused by abnormal angiogenesis generating larger gaps in endothelial tissues, to increase the delivery of nanoparticles, drugs and other non-targeted molecules to tumors. From initial injection, the nanoparticles must traverse the circulatory system. The first hurdle for the nanoparticles would be macrophage targeting which can result in a major loss in injected dose exceeding 50% within a few hours[53]. Protein binding during circulation is the primary method for macrophages such as Kupffer cells from the liver to target nanoparticles[53]. Larger particles are more likely to be targeted by the liver and removed from circulation (upper limit is 300 nm)[1,2] as are charged particles. Typically for in vivo studies coatings like such as PEG are used to protect the nanoparticles by changing the surface characteristics[54]. While larger

particles are targeted by the liver, small nanoparticles are more likely to be filtered through the kidney. Particles smaller than 6 nm and up to 9 nm have been shown to filter out of the body rapidly due to the kidney[55]. The next major hurdle is the diffusion of the nanoparticle through the endothelial layer and through the tumor region itself. While the gaps are larger in the endothelial layer in tumors than healthy tissue, the size of the nanoparticles determine the effectiveness of crossing through endothelial gaps[56]. Larger particles diffuse through less readily than smaller ones. Additionally, once the particles enter the tumor, they must travel through the extracellular matrix a greater distance than 100 um to enter hypoxic regions. Smaller nanoparticles have been shown to diffuse more readily throughout the extracellular matrix as well[57]. The overall effectiveness of in vivo accumulation in the tumor region has been determined to be between 10-12nm as the nanoparticles are the smallest size possible that avoids kidney filtration and passive diffusion into healthy tissue while maximizing the diffusive properties in tumor regions[2]. Although 10-12 nm nanoparticles are ideal for in vivo tumor accumulation, the size is not ideal for cellular accumulation. Additionally, while the EPR effect has been relied upon for tumor targeting, it has proven to generate insufficient accumulation of nanomaterials for studies to translate from in vivo models to clinical trials.

A study published in Nature comparing 45 studies specifically for gold nanoparticles, varying in size, it was found that an average of only 1% intravenously injected gold accumulated in the tumor[6]. The study goes on to suggest that even a two fold increase in accumulation would greatly improve the prospects of gold enhanced radiation therapy, which this study aims to demonstrate with the use of ultrasound stimulated microbubbles.

1.5 Ultrasound stimulated Microbubbles

Microbubbles are gas bubbles, usually coated with lipid or protein shells that were primarily designed as ultrasound contrast agents[15]. As the name suggests, they are micrometers in diameter, usually ranging from 1-10 um. The gas core provides a different medium for the sound to travel, causing increased scattering of ultrasound waves, increasing contrast in regions with bubbles, usually the blood

stream. Additionally, the gasses used are usually rather heavy with low diffusion and the shells that coat the gas both improve stability[58]. The improved stability allows the microbubbles to remain intact when stimulated by ultrasound, undergo oscillations. The oscillations increase backscatter further improving the signal strength generated as the ultrasound wave transmits through a medium [59].

1.5.1 Microbubble Activity

Microbubbles behave differently depending on the frequency, pressure of the ultrasound field they are exposed to. Primarily based on size, microbubbles have a resonance frequency in the ultrasound range. The close the transmitted ultrasound wave is to that resonance frequency, the more energy is transferred to the microbubble, although the microbubbles will still respond to other frequencies outside of resonance. When microbubbles are exposed to low pressure ultrasound waves, they respond by oscillating to the transmitted frequency. Microbubbles will oscillate at the frequency of the transmitted wave, where the high intensity peaks correspond to the compression of the bubble while the rarefaction results in microbubble expansion. The extent of the expansion and contraction tend to be comparable at low pressures thus it has been referred to as linear oscillation or cavitation. Under these conditions, the oscillating bubble is considered stable as the microbubbles do not collapse. Linear cavitation has the bubbles oscillating in to the frequency of the transmitted wave, thus generating a scattered signal primarily at the transmitted frequency.

As the pressure increases, bubbles display oscillating behaviors outside of the linear regime. The gas filling the microbubbles can only be compressed so far, while the expansion is less limited. The bubbles begin expanding greater than they contract, and as a result the oscillations become nonlinear. Asymmetrical behavior causes backscatter at not only the transmitted frequency, but also at higher order harmonics and ultra-harmonics. Under these conditions the microbubbles can collapse from the inertia of the liquid. The collapse of these microbubbles generates a shockwave leading to a large and rapid broadband signal[60]. Additionally after collapse short lived bubbles are formed from the escaped gas and can respond to the ultrasound wave as well. This form of oscillation is referred to as inertial or nonlinear

cavitation. The nonlinear response that characterizes inertial cavitation generates scattered signals at higher harmonics as well as ultra-harmonics signals.

1.5.2 Integrated Cavitation Dose

One method of measuring and characterizing bubble activity, and the one used in this study, is passive cavitation detection (PCD). By passively listening to the scattered signal from oscillating bubbles using a second transducer, the type and magnitude of the response to ultrasound can be ascertained. Changing the passively recorded signal to the frequency domain using a Fourier Transform, the strength of the signal across a range of frequencies can be analyzed. A typical method of analysis is the integrated cavitation dose (ICD) where the area under the Fourier transform is calculated to develop insight into bubble behavior[61]. The area can be analyzed in from different bounds or by an overall broadband signal to obtain general or more specific information about the bubble activity. Inertial cavitation will have a more nonlinear responses due to the uneven expansions compared to contractions and due to the broadband signal emitted form bubble collapse, meaning that the area bounded across higher harmonics will be greater[62]. In general, the greater the ICD the more bubble activity is occurring and the greater the area under higher harmonics, the more inertial cavitation present.

1.5.3 Bioeffects of USMB

1.5.3.1 Sonoporation

While microbubbles are designed to enhance contrast in ultrasound images ultrasound contrast, when used at therapeutic ultrasound conditions, they can trigger biological effects. When cells are within close proximity of microbubbles as they oscillate from exposure to an ultrasound field, the cells experience temporary enhancement of cellular accumulation, of both permeable and impermeable surrounding molecules. This phenomenon has been broadly called sonoporation and is a major focus of this study[63].

The mechanisms associated with USMB enhanced cellular accumulation is yet not fully understood. One mechanism is the generation of transient pores on the cellular membrane based on observations that cells can generate openings of various sizes in the cell membrane when exposed to an

USMB. The pores have been observed to be as large as 100nm under specific circumstances while still being repairable[21,64]. It is possible to generate pores too large to repair, resulting in cell death. The formation of pores allows membrane impermeable molecules to passively diffuse into cells. Molecules like calcium ions, which have been linked to other bioeffects induced by USMB, and Propidium Iodine have been shown to accumulate in cells after ultrasound and microbubble treatments[22]. These pores that open by USMB are repaired by the cells shortly after exposure, in the order of minutes[65].

Additionally, others have demonstrated that USMB treatments enhance accumulation by stimulating endocytosis. Catherin based endocytosis have been shown to have increased rates for a period shortly after the ultrasound treatment[26]. Additionally fluid phase uptake is also enhanced. These enhancements occur for around 30 to 60 minutes after treatment[20,65].

1.5.3.2 Radiation therapy enhancement

Ultrasound and microbubbles, in addition to causing cells to have enhanced accumulation of surrounding molecules can cause other beneficial bioeffects. In tumors, it has been shown that the vascular disruption caused by ultrasound stimulated microbubbles increases the efficacy of radiation treatments to a tumor[66]. Evidence supports that ultrasound and microbubbles increase the expression of ceramide, most likely due to membrane stress[18,66,67]. Although the mechanism is unclear, ceramide has been linked to cell death, particularly with vessel disruption and during ultrasound and microbubble treatments in tumors, it has been shown to have increased expression levels. Both Caspase9-alpha and caspase9-beta, which are linked to apoptosis pathways, were shown in vitro to greatly increase in expression after a combined ultrasound microbubble and radiation therapy treatment, but not each treatment separately[67–69].

1.5.4 Mechanism

The way microbubbles stimulate these bioeffects is also not completely understood. The rapid oscillations of the microbubbles can generate microstreaming around it. The streaming liquid is thought to generate sheer stress on the membrane, which in turn possibly triggers mechanosensors on the

membrane, along with by interfering with actin inside the cell, stimulating endocytosis pathways [25]. Another possible mechanism could be the stress placed on the membrane by pulling and pushing from the expanding and contracting of the microbubbles when microbubbles are in very close proximity to the cell wall. The stress too, can cause pores or stimulate endocytosis. As ultrasound pressures increase, the amplitude of oscillation increases, causing more microstreaming and overall more stress in general[18]. As a result, it has been observed that as pressure increases, the net accumulation of molecules increases as well until cells begin to lyse[19].

Lastly, micro jets can form when a microbubbles collapses under violent oscillations such as in inertial cavitation. When microbubbles contract near a ridged surface, pressure on the bubble is uneven (as the ridged wall does not apply pressure while surrounding liquid does), generating a net pressure from the top of the bubble towards the ridged surface. The surrounding liquid can follow the path of the net pressure, collapsing the bubble and generating a microjet perpendicular to the ridged surface. It has been theorized that micro jets puncture the cell membrane generating pores during inertial cavitation[70]. It has even been suggested that reactive oxygen species generated by collapsing microbubbles can contribute to modulating protein channels on the cell membrane, increasing uptake[71]. Figure 1-4 demonstrates the various methods of enhanced accumulation. The enhancement in cellular accumulation is thought to be proportional to ultrasound pressure. This study will attempt to improve cellular accumulation of gold nanoparticles by utilizing the enhanced accumulation bioeffects caused by ultrasound induced microbubbles.

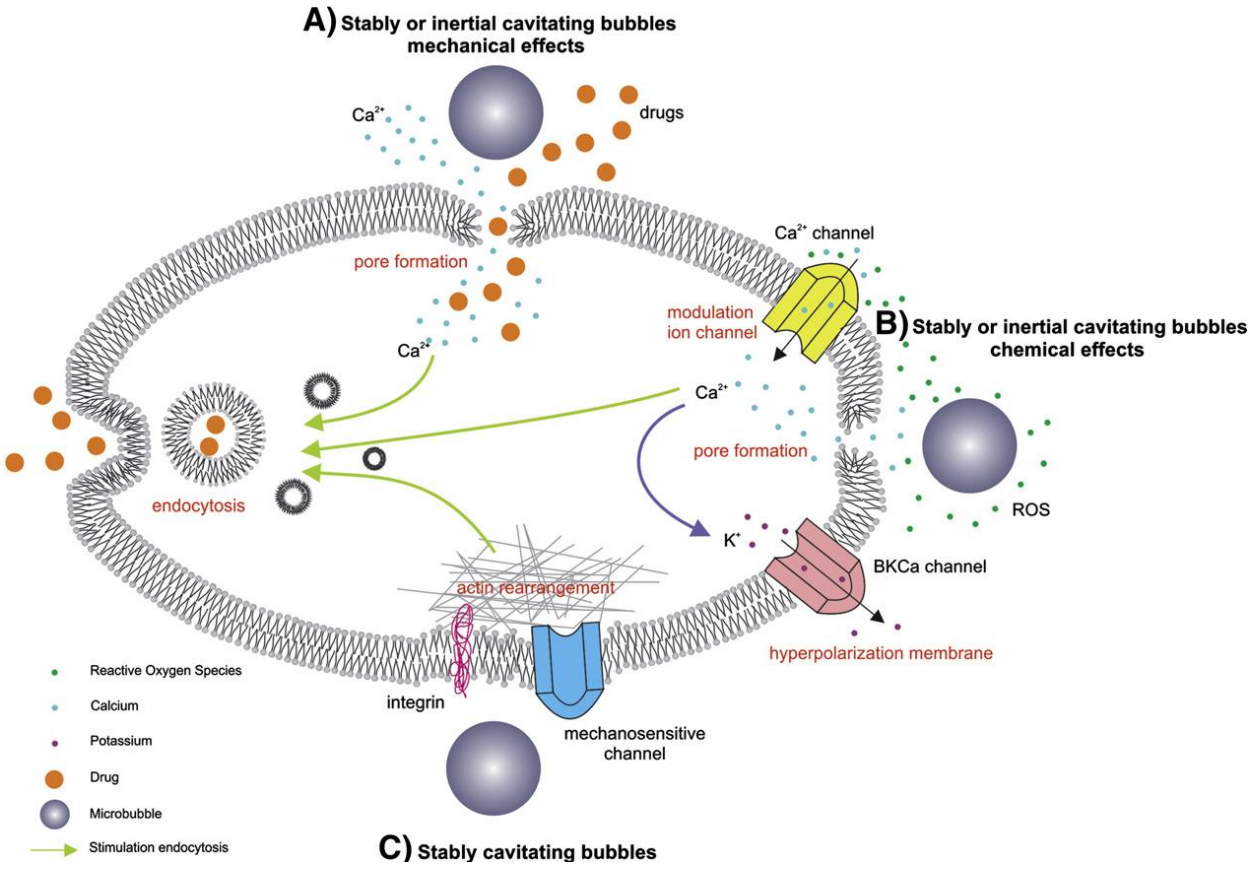

Figure 1-4[18]: Potential Biological effects of stably and inertial cavitating microbubbles with regards to accumulation. (A) Stress on the membrane from pushing and pulling forces during microbubble oscillations can potentially generate pores, allowing for diffusion (B) The production of reactive oxygen species from oscillating bubbles can interact with membrane lipids disrupting them and can modulate ion channels. (C) Microstreaming generated by stably cavitating bubbles generates shear stress on the membrane triggering mechanosensores, and interfering with actin, which may lead to increased endo and exocytosis rates. Additionally, the calcium influx triggered by pore formation is linked to endocytosis.

1.6 Hypothesis

Radiation therapy, while commonly utilized clinically to combat tumor growth, is hindered by the dose limitations to surrounding unaffected tissues. Methods that increase local radiation dose, such as radiosensitizers like gold nanoparticles are one way to overcome radiation therapy's inherit limitations, although they have their own difficulties as well. Because AuNP radiation enhancement has a large dependence on Auger electrons which deposit energy within 200 nm, target proximity and nanoparticle size are factors that affect radiosensitization, along with total gold accumulation within a target region. Thus gold nanoparticle assisted radiation therapy is limited by cellular accumulation and proximity to DNA. Ultrasound stimulated microbubbles are known to increase cellular accumulation of surrounding

molecules by improved rates of endocytosis and pore formation. Additionally diffusion through pores may allow gold nanoparticles to avoid endosomal entrapment, potentially facilitating nuclear targeting of NLS functionalized nanoparticles.

This study will examine whether USMB can provide greater therapeutic benefit to gold nanoparticle assisted radiation therapy by increasing cellular accumulation and by allowing nuclear targeting of functionalized nanoparticles. The main objectives of the study are to measure cellular gold concentration with and without USMB, to determine whether NLS labeled nanoparticles have entered the nucleus after USMB treatments and if the efficacy of AUNP+XRT is improved when adding USMB by clonogenic assay.

2 Methodology

2.1 Cell Culture:

PC3 prostate cancer cells were chosen as a relevant cell line for this study. PC3 were grown with Roswell Park Memorial Institute (RPMI) 1640 media supplemented with 10% Fetal Bovine Serum at 37^0C with 5% CO_2 with passages at 70-80% confluence. Cell passage was performed with 0.25% trypsin incubated with the cells for 4 minutes, followed by centrifugation at 100 g to remove excess trypsin and re-suspended in media. Prior to experiments, cells were re-suspended with a cell concentration of 2 million cells per mL.

2.2 Definity Microbubble Activation

Definity (Lantheus Medical Imaging, Billerica, MA, USA) microbubbles were activated once at room temperature by shaking using Vial-Mix (Lantheus Medical Imaging, Billerica, MA, USA). The vial was inverted and was let rest for 5 min to achieve equilibrium. The vial was vented with an 18 Gauge needle while 500 uL of microbubbles were extracted with another 18 gauge needle with a syringe. The Definity microbubbles were diluted in a 1:1 ratio with Phosphate Buffer Saline into another syringe and mixed by hand. About 50 uL of the solution was added to each sample immediately prior to treatment achieving a V/V ratio of 1.7%. The stock concentration of Definity has on average 1.2 $x10^{10}$ bubbles/mL ranging from 1.1-3.3 um in size. The final concentration is 2 x 10^8 ub/mL, with an approximate bubble to cell ratio of 33 ub per cell within each sample.

2.3 Ultrasound treatment:

Ultrasound treatments were performed in a water tank with submerged transducers. The emitting transducer, a 1.0 MHz (IL0202HP, Valpey Fisher Inc., Hopkinton, MA) center frequency transducer (diameter = 42 mm; focal length = 4.8 cm; beamwidth = 2.0 mm) was used for the treatment while a 2.25 MHz (IL0208HP, Valpey Fisher Inc., Hopkinton, MA) center frequency transducer (diameter = 25 mm; focal length = 8 cm; beamwidth = 2.0 mm) was used as a passive transducer to detect microbubble activity during ultrasound treatments. A volume of 3 mL of 2 million cells per mL were added in

suspension to a cylinder with acoustically transparent walls. Both 9 μg of AuNP of either 10 nm, 50 nm or 10 nm with additional NLS coating, and 1.7% V/V ratio of Definity microbubbles were added to the cells within the chamber. The chamber was then submerged in a water tank for treatment. The emitting transducer placed at the focal distance treated the sample at 47.5, 75 or 100 mV corresponding with acoustic peak negative pressures at the center of the treatment volume of 370, 570 and 770 kPa respectively. The emitting transducer treated the sample with 8 cycles at 1 MHz with a pulse repetition frequency of 500 Hz. The passive transducer placed at focal distance perpendicularly to the emitting transducer relative to the treatment chamber recorded the signal for the 30s duration.

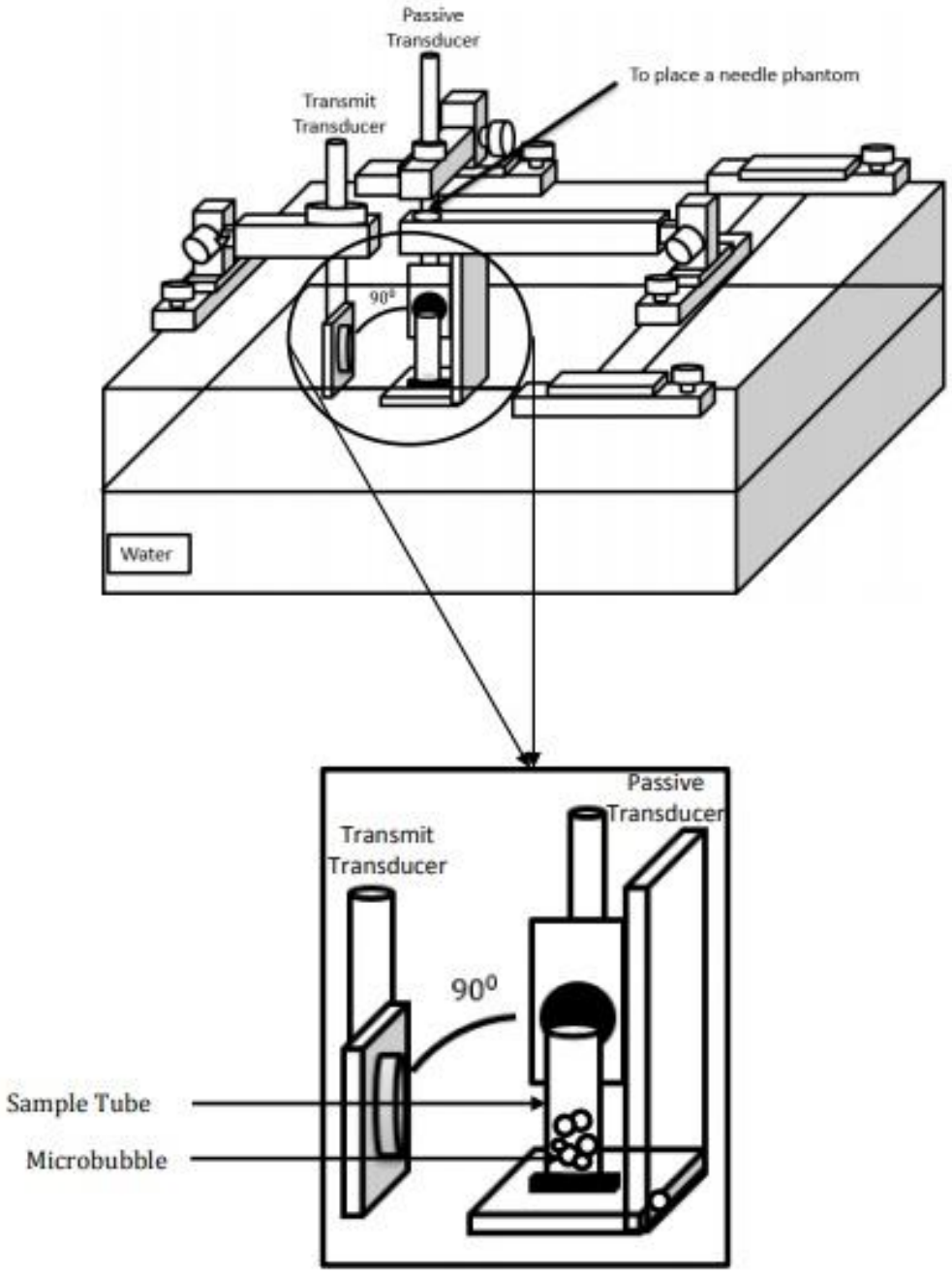

Figure 2-1(Adapted From Shadab Momin): Schematic diagram of experimental set up, with transmitting transducer perpendicular to the passive transducer, both facing the acoustically transparent mylar chamber

Once the sample was treated, it would be removed from the chamber and placed in a tube to incubate for 3 hours. The sample would be kept in suspension by gently shaking the sample every 10 min for the 3 hour duration. After incubating with the AuNP for 3 hours, the sample would be centrifuged at

100 g for 4 min to remove remaining AuNP. The sample would be re-suspended again in PBS and centrifuged once more.

2.4 Integrated Cavitation Dose (ICD):

The passive transducer recorded the echoed response from the microbubbles in the chamber in 50 μs sections every 2 ms. The acquired data corresponded to 15 000 separate sections. A Fast Fourier transform was applied to all 15 000 signals to convert to a frequency domain. The Power Spectrum was converted from the Fourier transforms and the area was calculated 500 kHz centred around 1, 2, 3 and 4 MHz then added together, and all 15 000 harmonic areas were summed. The background signal was integrated in the same manor and subtracted from the integrated values to obtain ICD

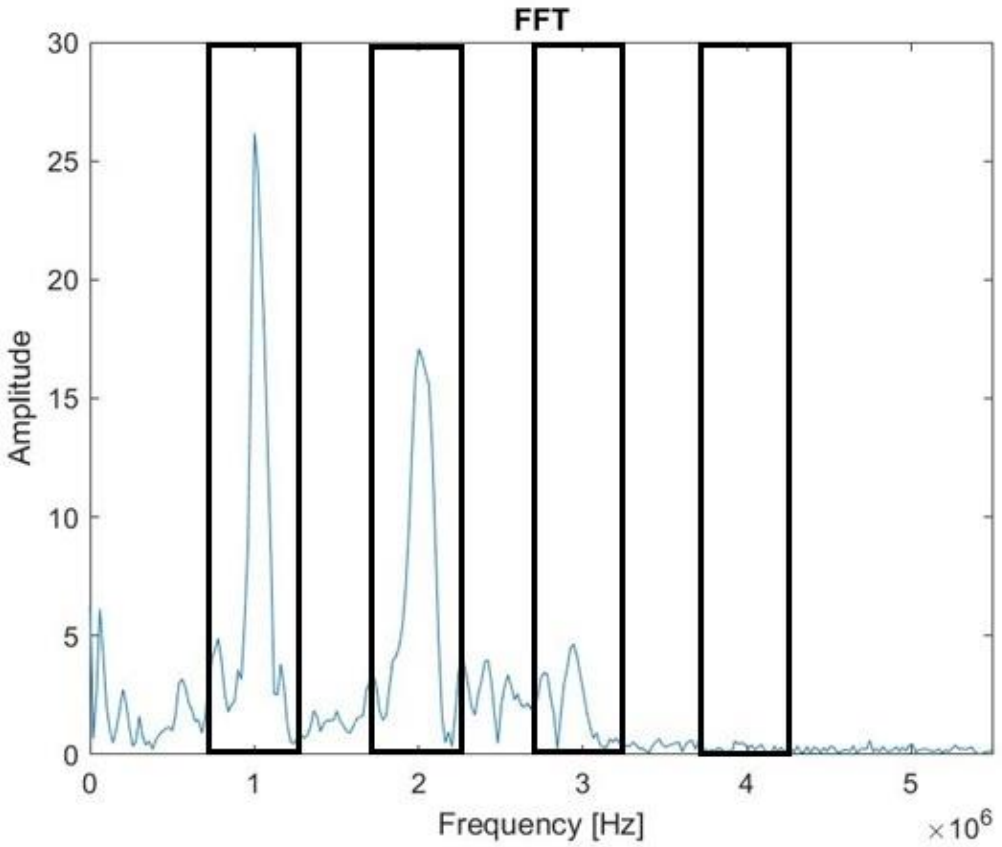

Figure 2-2: Arbitrary Amplitude vs. Frequency of a single 8 cycle ultrasound pulse with a peak negative pressure of 770 kPa, recorded at 15 seconds during treatment. The signal was transformed with a Fast Fourier Transform (FFT) to obtain the figure above. The Fourier Transform was then integrated and added with the bounds of 500 kHz centered at 1, 2 3 and 4 MHz (black rectangles). The values obtained across each of the 15 000 signals in a 30 s treatment were added to obtain a total ICD

2.5 Gold Nanoparticle Mass Quantification

Gold quantification was performed with ICP AES at the University of Toronto Analest lab. Prior to measurement each sample was treated with 1 mL of aqua regia at a 4:1 ratio of HCL and HNO_3 for 1-2 hours while in a hot water bath at about 100^{o}C. Once the sample cells were dissolved it was forced through a 0.22 μm filter and diluted with distilled water. It was then measured using the ICP AES.

2.6 Radiation therapy

Cells were treated at the same conditions as the ultrasound treatment, except that only a peak negative pressure of 770 kPa was used and an ultrasound alone sample was added. After treatment and 3 hours of incubation, excess gold was removed by centrifugation. From each sample 1 million cells were plated into a well on a 6 well plate and were allowed to settle on the bottom for 1-2 hours. The cells were then irradiated with 2 Gy of 225 kVp ionizing radiation by XRAD at STTARR lab, removed from the well with 0.25% trypsin and plated for colonies at concentrations of 100 or 300 cells for untreated and treated respectively.

2.7 Clonogenic assay

After treatment with 2 Gy of XRT, survival fraction was measured using clonogenic assay. Cells were plated in 6 well plates and incubated 14 days. The cells were then stained with 1% Methylene blue and colonies greater than 50 cells were counted. Average clonogenic viability (V_c) represented as a survival fraction was determine from a population set n=12.

2.8 Data Analysis

2 way Anova was used to determine statistical significance within and between the different types of AuNP, for accumulation and viability. Multiple comparison tests were used to determine the P values between sets, where $P<0.05$ was considered significant. R squared values were obtained to assess the linear correlation between ICD values and cellular accumulation. Synergism was determined using the Bliss criteria, where additive survival fractions (V_a) were determined by multiplying survival fractions of two effects were compared to the V_c. The combined treatment was considered synergistic when V_c was lower than V_a.

3 Results

This study demonstrated the notion that USMB enhances AuNP uptake in PC3 prostate cancer cells, resulting in enhanced radiosensitivity. In addition, the results indicate a positive relation between cellular uptake and bubble activity, with the most significant increases occurring past the inertial cavitation threshold according to ICD. Furthermore, when comparing accumulation of different AuNP sizes, the optimal size is 50 nm in all conditions, also showing greater improvement at 370 kPa. The combined treatment of USMB and AuNP has shown to improve the accumulation of AuNP by up to 3 fold and synergistically improve XRT with all particles, with optimal results occurring with 10 nm NLS nanoparticles treated at 770 kPa combined with XRT showing above a 5 fold increase in treatment efficacy when compared to XRT alone.

3.1 USMB enhanced uptake of Gold nanoparticles

The enhancement of radiation therapy by AuNP is dependent on the internalized AuNP concentration. The ability of USMB to enhance accumulation of AuNP of various sizes into cells was assessed through quantification of AuNP mass accumulation within cells at varying ultrasound pressures (370, 570 and 770 kPa) in order to ascertain optimal conditions and nanoparticle type. Cells exposed to 9 mg/kg of PEGylated gold nanoparticles with sizes of 10 nm, 50 nm and 10nm with a NLS were treated with 1 MHz ultrasound 30s at pressures of 370 kPa, 570 kPa or 770 kPa. Figure 3-1shows the uptake in mg per cell across all ultrasound conditions for each nanoparticle type.

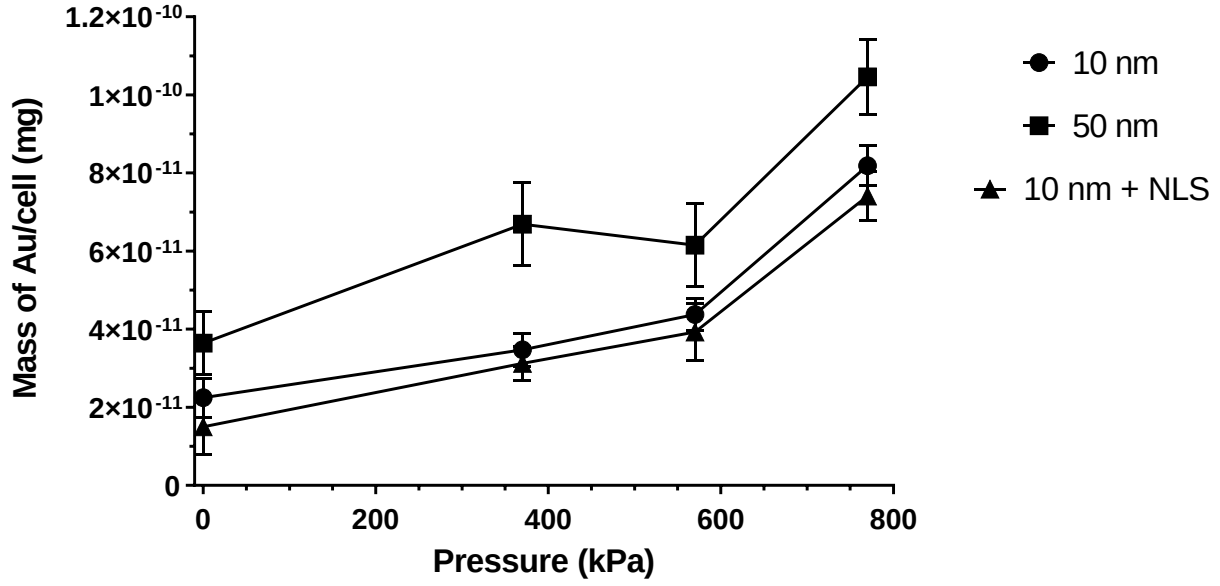

Figure 3-1: Mass of AuNP per cell in mg vs. Acoustic Pressure. Mass of PEGylated AuNP measured by ICP-AES for 50 nm, 10 nm and 10 nm with NLS. Ultrasound treatments were done with a 8 cycle, 1 MHz wave repeating every 2 ms for a total duration of 30s.

Figure 3-1 displays a positive correlation between AuNP uptake and pressure for all the different types of nanoparticles, with the greatest increase in uptake for all particles occurring at 770 kPa, all of which were statistically relevant (P value<0.0001). When combined with USMB with a pressure of 370 kPa, the cellular accumulation of 50 nm AuNP increases greatly from $3.64 * 10^{-11}$mg/cell to $6.69 * 10^{-11}$mg/cell, nearly a 2 fold increase in accumulation, while notably, 10 nm only increased from $2.25 * 10^{-11}$ to $3.47 * 10^{-11}$mg/cell. For the 50nm particles, the uptake increased in the presence of USMB at all pressure conditions (P value < 0.0001) but did not show a significant deference between 370 and 570 kPa (P=0.9964).

The 10nm AuNP showed no statistical difference between untreated and 370 kPa (P=0.3706), and between 370 kPa and 570 kPa (P=0.8016), although on average there was an increase with ultrasound pressure. The 10nm with NLS did see statistical difference between untreated and 370 kPa (P=0.0244) but not between 370 and 570 kPa (P=0.8959). It was apparent however that 770 kPa treatments had statistically more AuNP per cell for both 10 nm and 10 nm NLS particles, with a maximum uptake of

$8.18 * 10^{-11}$mg/cell and $7.41 * 10^{-11}$mg/cell respectively. Between the 10 nm and 10 nm NLS nanoparticles, while on average the addition of NLS lowered accumulation slightly, there were no significant statistical differences between them in all conditions (P>0.05), suggesting that size is a far greater contributor than the NLS signal for accumulation. Between the 10nm particles with and without NLS and the 50nm particles, the 50 nm particles showed greater uptake in all conditions, with maximum cellular accumulation of $1.05 * 10^{-10}, 8.18 * 10^{-11}$ and $7.41 * 10^{-11} mg/cell$ for 50 nm, 10 nm and 10 nm NLS respectively; occurring at 770 kPa in all instances.

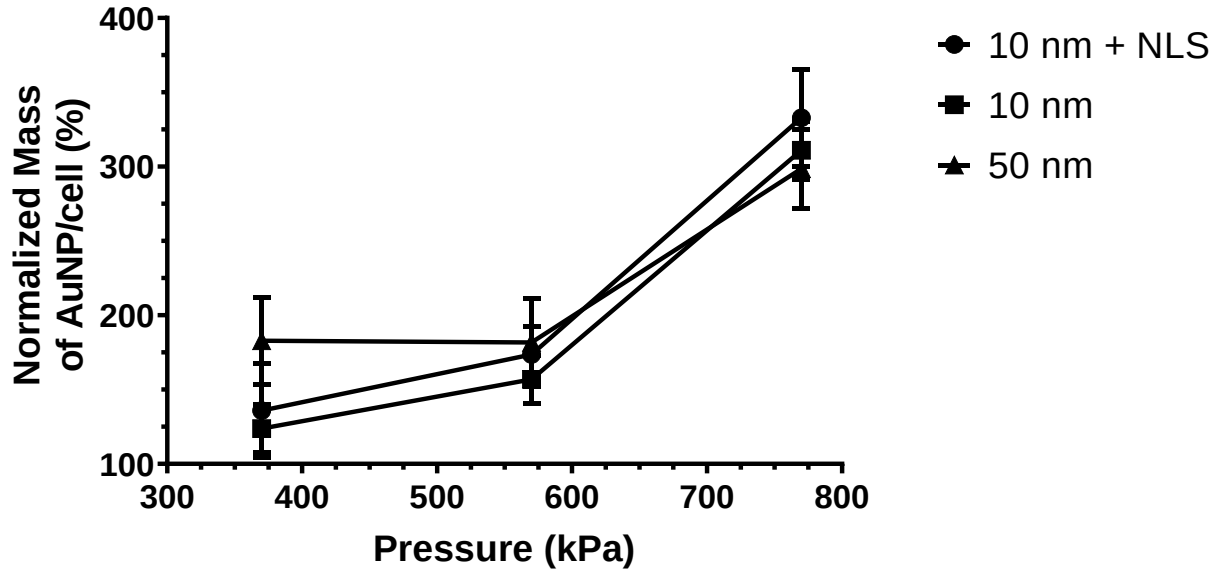

Figure 3-2: Normalized Mass of AuNP per cell vs. Acoustic Pressure. Mass of PEGylated AuNP measured by ICP-AES for 50 nm, 10 nm and 10 nm with NLS. Mass values were normalized to USMB negative samples (set to 100%) per repetition prior to averaging. Ultrasound treatments were done with a 8 cycle, 1 MHz wave repeating every 2 ms for a total duration of 30s.

Figure 3-2 displays the accumulation of AuNP mass normalized to each type of AuNP in the absence of USMB. We see that USMB can increase cellular accumulation of all the tested AuNP at most by approximately 3 fold (333%, 311% and 299% for 10 nm with NLS, 10 nm and 50 nm respectively) at pressures of 770 kPa. The largest difference between the AuNP types occurs when treating at 370 kPa, where the 50 nm AuNP achieve an improvement to 183%, statistically higher than the improvement to 10

nm AuNP of 126% (P=0.005). Comparing the relative accumulated mass of all the nanoparticle types we find that there is no significant statistical difference between the nanoparticles at conditions exceeding 370 kPa (P>0.05).

The next objective was to determine if the cavitation activity associated with USMB treatment was related to cellular accumulation of AuNPs. Bubble activity was quantified using Integrated Cavitation Dose, or ICD as described in the methods, measured using a passive cavitation detection system. Figure 3-3 displays ICD across the pressures used. ICD is measured in arbitrary units as the passives signal's magnitude is dependent on experimental setup, and as such is used for comparison across ultrasound conditions only.

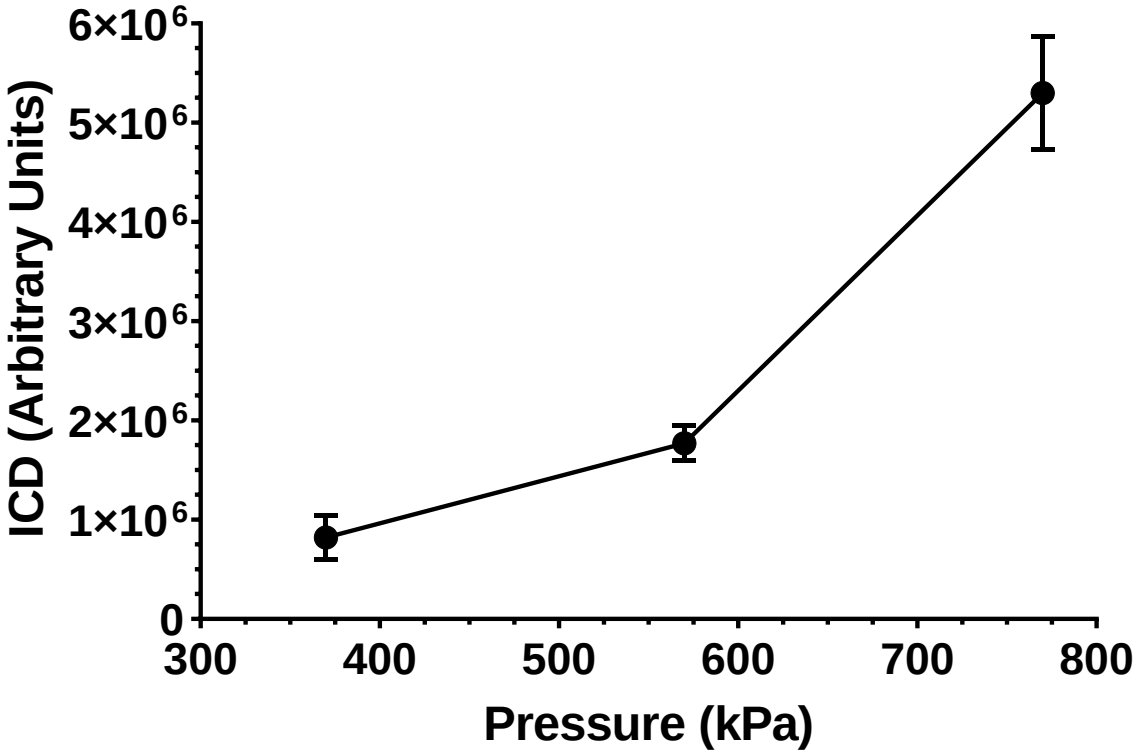

Figure 3-3: ICD vs. Pressure (kPa) for ultrasound treatments with cells at 370, 570, and 770 kPa. Samples were treated with 8 cycles of 1 MHz ultrasound repeating every 2 ms for 30s. The ICD values were obtained via passive cavitation detection, integrating under the power spectrum at 500 kHz range under 1-4th harmonics and adding them. This was done for all 15 000 pulses and added together.

From figure 3-3, it is evident that ICD values increase with pressure suggesting greater bubble activity at higher pressures. ICD went from $0.82 * 10^6$ to $1.77 * 10^6$ from 370 kPa to 570 kPa. But from 570 kPa to 770 kPa, we see a much larger increase in ICD, going from $1.77 * 10^6$ to $5.30 * 10^6$, suggesting a significant change in bubble activity at 770 kPa. The relationship between bubble activity and cellular accumulation shown in figure 3-4 compares the AuNP cellular accumulation in mass, to the ICD (summed across $1^{st} - 4^{th}$ harmonics and across 30 s of treatment). As ICD increased, the cellular accumulation increased in a linear fashion. The R squared values of 0.97, 0.80, and 0.93 for 10 nm, 50 nm, and 10 nm with NLS respectively suggest that there is a direct positive correlation between ICD and cellular accumulation.

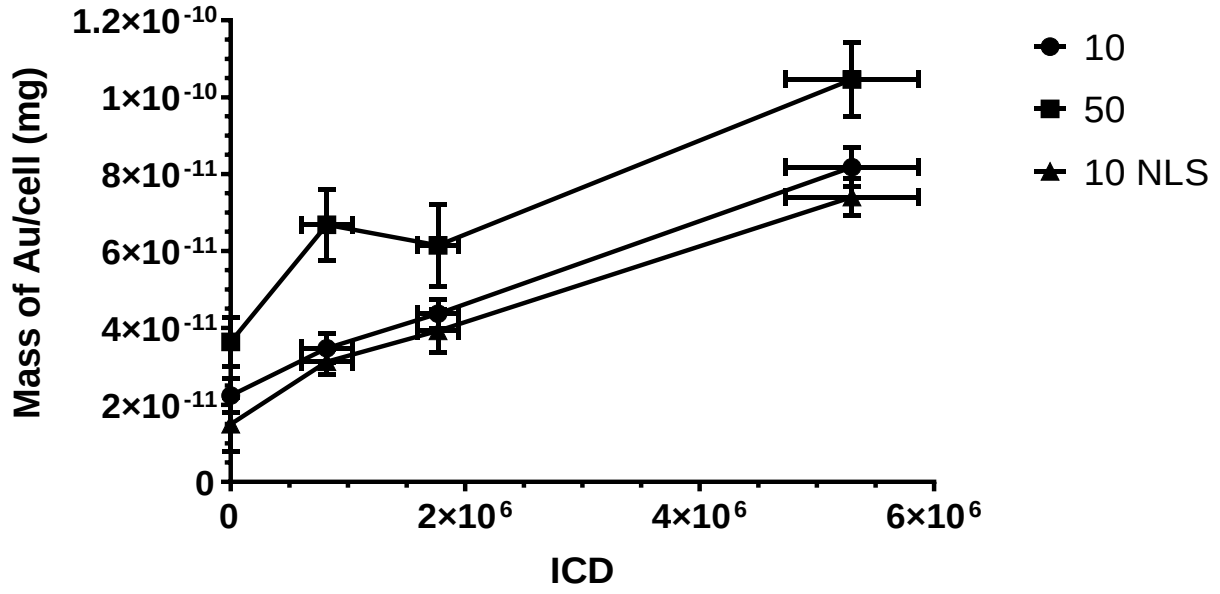

Figure 3-4: Mass of AuNP per cell in mg vs. ICD (arbitrary units). Mass of PEGylated AuNP measured by ICP-AES for 50 nm, 10 nm and 10 nm with NLS. Ultrasound treatments were done with a 8 cycle, 1 MHz wave repeating every 2 ms for a total duration of 30s. ICD values were calculated by integrating with a range of 500 kHz centred on the 1^{st} to 4^{th} harmonics and adding them. This was done for all 15 000 pulses and added together.

3.2 Viability:

While AuNP accumulation is improved by USMB due to enhanced microbubble activity, the improvement to XRT needs to be considered. The next objective of this study was to determine if USMB

enhances radiation therapy of AuNP+XRT and if so, which type of nanoparticle improves XRT efficacy the greatest and how it might relate to accumulation. By using clonogenic assay to determine survival fractions (V_c) after XRT under different conditions, it is possible to determine the degree enhanced accumulation of Gold nanoparticles benefits radiation therapy and whether or not USMB has a synergistic effect in conjunction with AuNP and XRT. Cells exposed to 9 mg/kg of PEGylated AuNP with sizes of 10 nm, 50 nm and 10nm with NLS were treated for with 1 MHz ultrasound for 30s at 770 kPa because it showed optimal accumulation with all nanoparticles out of the conditions tested in this study. After 3 hours of incubation, excess AuNP were removed then cells were irradiated with 2 Gy at a potential of 225 kVp and plated for clonogenic assays. Figure 3-5 shows the survival fraction normalized to the untreated control for the cells alone, and cells incubated with the different nanoparticles treated with USMB, with XRT and both USMB and XRT .

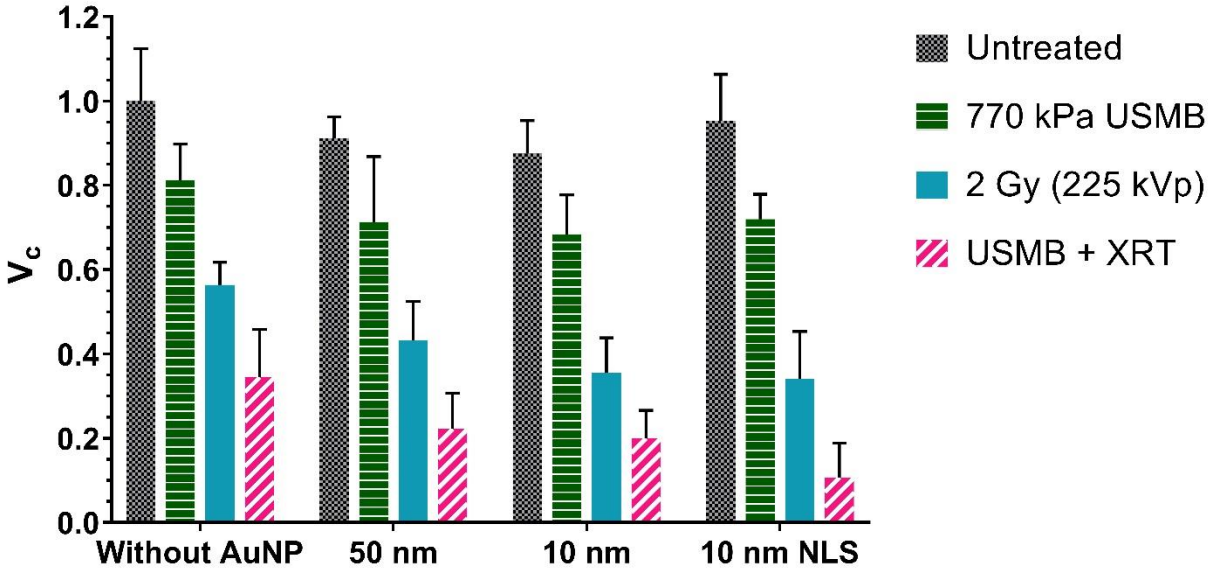

Figure 3-5: Survival fraction of Pc3 cells at different conditions. 9 mg/kg of AuNP were added for each of the AuNP samples regardless of size while the ultrasound conditions that were used were for the appropriate samples was 770 kPa. The radiation treatments used for the radiation positive samples was 2 Gy treated at 225 KeV.

From figure 3-5, we can see that for all types of nanoparticles, the greatest reduction in viability occurred when combining USMB and XRT, with average survival values of 0.22, 0.20, and 0.11 for 50 nm, 10 nm, and 10 nm with NLS respectively. On average 10 nm with NLS improved efficacy the most, greater than 5 fold when combined with USMB and XRT, although there was no statistical difference between the different nanoparticles when combined with USMB and XRT ($P>0.05$). For all AuNP types used, it was found in figure 3-5 that the resulting decrease in cell viability from AuNP+USMB+XRT was synergistic when compared to XRT and USMB+AuNP alone with the Bliss calculated additive survival fraction (V_a) for XRT and USMB+AuNP as 0.40, 0.39 and 0.41 compared to 0.22, 0.20 and 0.11 for 50 nm, 10 nm and 10 nm with NLS respectively. Additionally, USMB + AuNP + XRT showed statistically lower results than AuNP + XRT alone for all three nanoparticle types, 0.43, 0.35, 0.34 compared to 0.22, 0.20 and 0.11 for 50 nm, 10 nm and 10 nm NLS respectively ($P<0.0001$).

USMB treatments without radiation showed a statistically different viability than relevant controls, both with and without AuNP ($P<0.0001$). USMB treatments with AuNP showed on average more death than without gold but there was no statistical difference ($P>0.05$). The addition of USMB without radiation reduced survival fraction by about 20% with and without AuNP. It is also worth mentioning that USMB combined with AuNP of all types did not synergistically improve cell death, comparing V_a of 0.74, 0.71, and 0.77, with the V_c of 0.71, 0.69 and 0.72 for 50 nm, 10 nm and 10 nm with NLS respectively. Additionally, there was no statistical difference between cell viability of USMB + AuNP of different nanoparticles ($P>0.05$). When combining USMB + XRT there is a decrease in viability as compared to either USMB alone or XRT alone. By the Bliss criteria, the V_a was found to be 0.46 for USMB+XRT, while the resulting V_c was measured as 0.35, showing synergism.

Comparing different AuNP effect on viability we can see that all nanoparticle types have minimal impact on cell survival at this concentration, with V_c of 0.91, 0.88 and 0.95 for 50 nm, 10 nm and 10 nm NLS respectively. Between each nanoparticle type there is no variation in survivability with no relevant statistical difference ($P>0.05$). When comparing AuNP + XRT, there is synergism for all nanoparticle

types when compared to XRT alone, with V_a of 0.50, 0.49 and 0.53 compared with V_c of 0.43, 0.35 and 0.34 for 50 nm, 10 nm and 10 nm NLS respectively. While there is no statistical difference between AuNP +XRT with each type of nanoparticle, it appears that on average the 10 nm particles show larger improvements to XRT efficacy, with 10 nm and 10 nm NLS nearly identical.

Lastly comparing USMB + AuNP + XRT for the different AuNP types, no statistical difference was observed. Although, unlike the AuNP + XRT treatments, it appears that on average 10 nm with NLS has shown a greater reduction to viability, V_c = 0.11 when compared to 10 nm, V_c=0.20 and 50 nm V_c=0.22.

Figure 3-6 compares the average of AuNP accumulation to average viability of each type of AuNP + XRT, with and without USMB. It is apparent that, although 50 nm AuNP have the greatest accumulation both with and without USMB when compared to 10 nm and 10 nm NLS, it does not reduce survival fraction more. Also, figure 3-6 displays the similarity between 10 nm and 10 nm NLS without ultrasound treatments, having similar uptake and viability measurements. Interestingly, when combined with USMB, 10 nm NLS particles seem enhance radiation better than 10 nm despite having slightly lower accumulation, although the values aren't statistically significant.

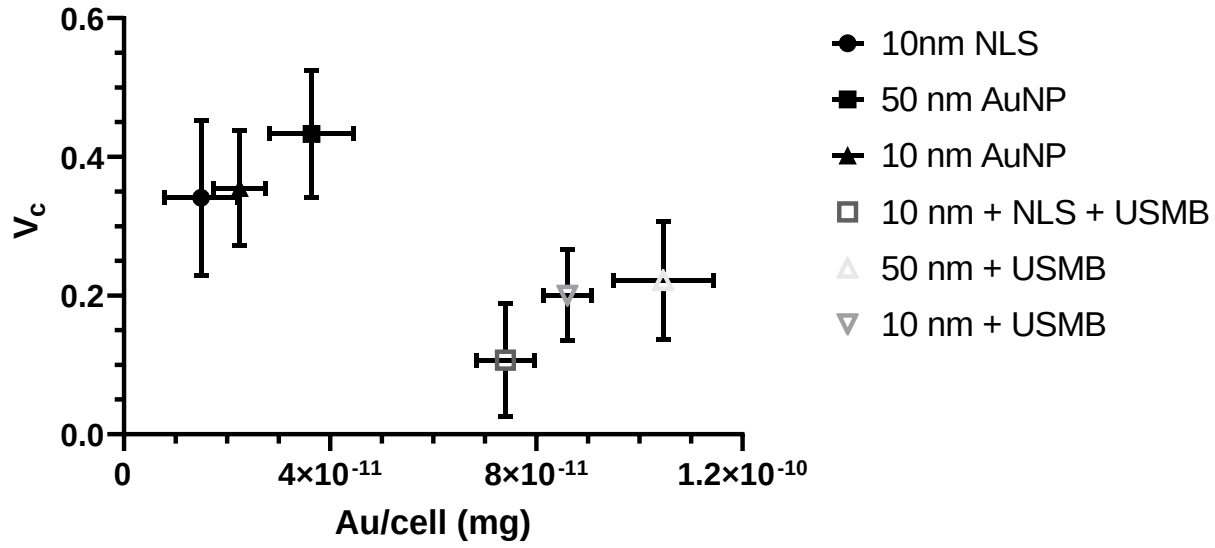

Figure 3-6: Clonogenic Viability measured in survival fraction vs. Mass of AuNP per cell in mg. 9 mg/kg of AuNP were added for each of the AuNP samples regardless of size while the ultrasound conditions that were used were for the appropriate samples was 770 kPa. The radiation treatments used for the radiation positive samples was 2 Gy treated at 225 KeV. ICP AES was used to measure AuNP content.

The last objective in this study was to determine if the greater radiation enhancement found in USMB + 10 nm with NLS AuNP + XRT was due to localization of the nanoparticles in the nucleus with USMB vs, without USMB. Figure 3-7 shows the images taken by a cytoviva hyperspectral camera with relevant reflectance spectral data of cells without the presence of AuNP, with 10 nm NLS with and without USMB.

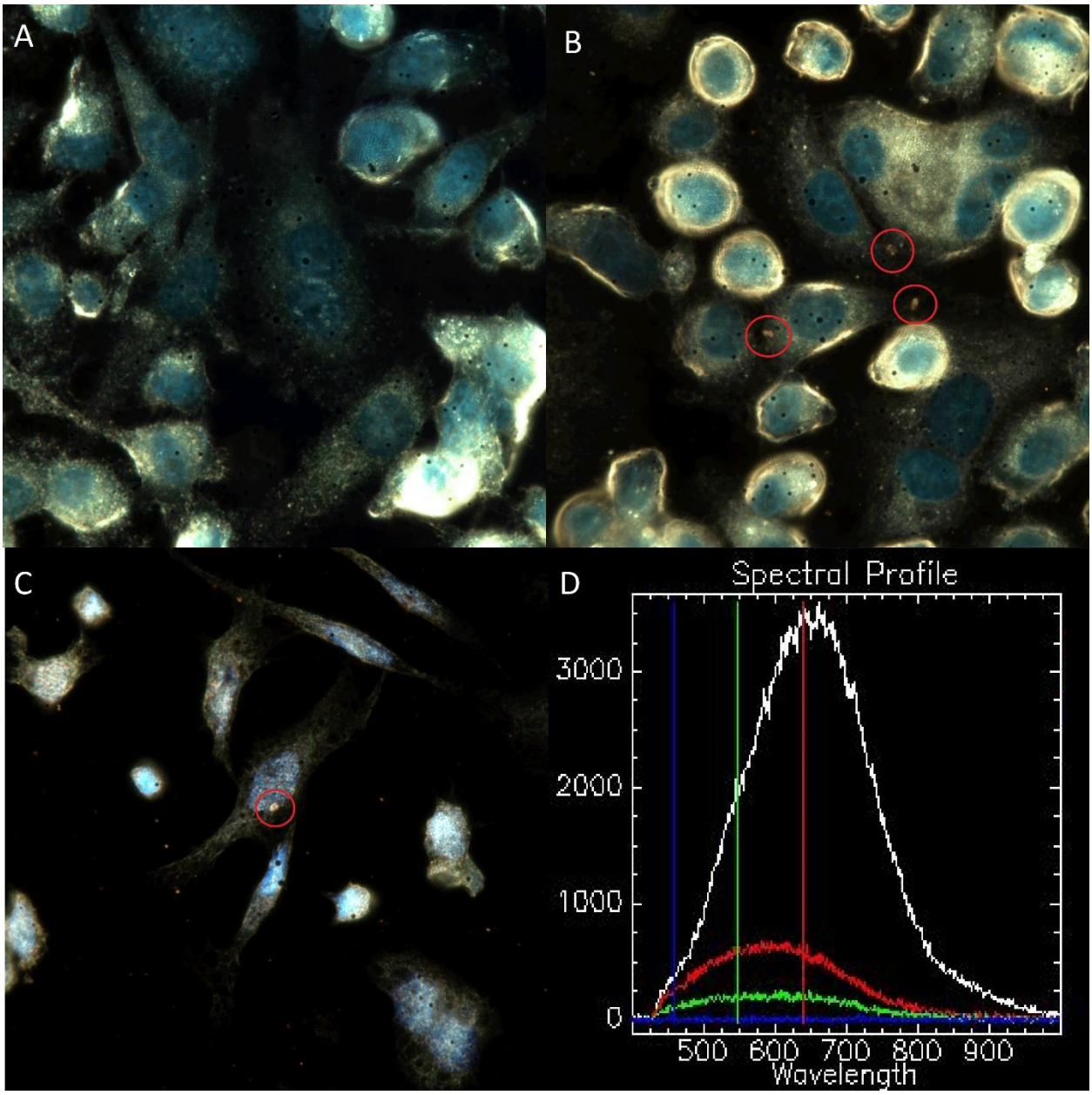

Figure 3-7: Hyperspectral image of A) PC3 cells alone B) PC3 cells incubated with 10 nm with NLS AuNP C) PC3 cells incubated with 10 nm with NLS AuNP treated with 8 cycles of 1 MHz 770 kPa ultrasound in the presence of microbubbles. Cells are stained with Hoechst to dye the nucleus, apparent as blue in the image. Images are taken at 100x magnification. D) Represents a typical reflectance spectra comparing Intensity (arbitrary units) at different wavelengths for individual pixels obtained from the cytoviva system. The white line is a spectra from AuNP with a high intensity peak with a peak near 670 nm, the red represents a bright part of a cell nucleus (peak about 600 nm), green represents the cytoplasm while blue is the background. The red circles indicate regions AuNP clusters determined by reflectance spectra.

Using the hyperspectral data measured by the cytoviva microscope, it is possible to determine the presence and location of metal nanoparticles within cells. The system measures the reflectance in a field of view which allows the use of AuNP's unique spectra from Surface Plasmon Resonance (SPR) to

visualize and identify the particles. Figure 3-7 B shows 10 nm NLS particles clustered within the cytoplasm, indicated within the red circle. The hyperspectral data displays peak reflectance around 670 nm with high intensity, consistent to what would be seen for metal nanoparticles. As shown by figure 3-7 D, the comparative spectra from the cell is different with a broader overall peak, which is closer to 600 nm. The USMB + 10 nm NLS sample also has a cluster of nanoparticles, with hyperspectral data similar to what is expected, with a specific peak near 670 nm. Qualitative observation of cell nuclei stained with Hoechst, represented by the blue hue, appears to indicate that there are some NLS nanoparticles overlapping with the nucleus when exposed to USMB and AuNP as opposed to AuNP alone, where the nanoparticles may be restricted to the cytoplasm.

4 Discussion

The results of this study demonstrate the synergistic effect of USMB in conjunction with PEGylated AuNP and XRT, with optimal results observed when using acoustic conditions that stimulate inertial cavitation and when using 10 nm AuNP with NLS. The combined treatment yielded greater than 5 fold reduction in viability in comparison to XRT alone, and over a 3 fold reduction in viability when compared to 10 nm AuNP with NLS treated with XRT without USMB. Additionally, the results yielded improvements in AuNP accumulation around 3 fold at inertial acoustic parameters for all three AuNP types. The results link for the first time to our knowledge, improvement in XRT efficacy with increased cellular accumulation of AuNP caused by USMB. This study has also demonstrated that USMB can possibly further improve the AuNP radiation enhancement by potentially facilitating nuclear localization.

4.1 USMB enhanced accumulation of AuNP

Limiting the clinical usefulness for AuNP combined with radiotherapy is the poor accumulation of AuNP within tumors. Additionally, the proximity of the nanoparticles to radiation sensitive targets, in most scenarios DNA, is important to obtain maximum improvements. Thus cellular accumulation becomes important. USMB has shown to increase the accumulation of molecules such as FITC[8] and Doxorubicin[72] among others, and for the first time to best of our knowledge AuNP accumulation has been measured directly through ICP AES when in combination with USMB. From our measurements, it is evident that 50 nm AuNP have the optimal accumulation both with and without the presence of USMB. It has been demonstrated that 50 nm AuNP have optimal cellular accumulation[4] due to favourable endocytosis rates, while smaller AuNP experience more exocytosis. The findings by Chithrani et al, compared extensively the effect of AuNP size on accumulation, finding that 50 nm AuNP nearly tripled in accumulation as compared to 10 nm[4]. While the treatments were conducted using constant concentration of AuNP for the various sizes as opposed to mass of gold like in this study, the established trend where 50 nm AuNP are optimal for cellular accumulation is still applicable.

When combined with USMB at 370 kPa, it is also evident that 50 nm AuNP showed the greater improvement in accumulation compared to 10 nm AuNP, nearly achieving a 2 fold increase from the untreated, statistically larger than the 10 nm AuNP which increased by about 30%. USMB has been shown to increase accumulation by both pore formation and enhanced endocytosis of various kinds, depending on the ultrasound parameters[24]. At low pressures generally understood to be below the inertial cavitation threshold, endocytosis is thought to be the largest factor in sonoporation[24,73] as shown by Deireppe et al. When treating cells exposed to SYTOX Green (a fluorescent molecule, 600 Da) with 200 kPa, they found the fluorescence intensity increased by 2.5 fold compared to when cells under the same conditions, had inhibited clathrin mediated endocytosis[24]. Due to the greater rate of endocytosis of 50 nm AuNP, further stimulating endocytosis would most likely have a greater impact on accumulation for 50 nm opposed to 10 nm which was observed at 370 kPa.

As pressures increased to 570 and 770 kPa, there was no change in relative uptake of 50 nm to both kinds of 10 nm AuNP, with maximum effect occurring at 770 kPa, with about a 3 fold increase for all particles. As pressures approach inertial cavitation regimes, pores begin to form allowing molecules to diffuse through the cellular membrane, the size of the pore increases with pressure[21,64]. As pressure hits inertial cavitation ranges, smaller molecules tend to diffuse more in cells[8]. Studies comparing the uptake of FITC of various sizes found that different mechanisms enhanced accumulation based on size. When comparing 4.4, 70 and 500 kDa FITC, Meijering et al found that when inhibiting endocytosis, 500 kDa FITC did not enter cells while the 70 kDa reduced in concentration and there was little impact on 4.4 Da FITC[17]. Additionally, a study done by De Cock et al, found that acoustic pressure positively correlated with uptake due to pore formation of FITC[19]. These findings support our results, as at higher pressure, the relative accumulation of 10 nm AuNPs of both types improved to be comparable to 50 nm, most likely due to the creation of, and diffusion through, membrane pores. Another study comparing FITC of different sizes, found that 10 kDa and 2 MDa molecules both experienced similar enhancements in accumulation when exposed to USMB[8]. Without the inhibition of specific uptake pathways, both sizes of

molecules, similar in size to the AuNP used in this study, were affected by USMB, further supporting the enhanced uptake seen for both sizes of AuNP. Therefore it is evident USMB greatly improves the cellular accumulation of AuNP of sizes between 10-50 nm by what is most likely a combination of endocytosis and pore formation. Additionally, there is no statistical difference ($P>0.05$) between accumulation 10 nm with and without NLS, both in value and trend, suggesting that size is a far greater contributor than the NLS signal for accumulation.

Biological effects of USMB have been linked with the magnitude and accumulative response of microbubbles to the acoustic field. The overall greatest bioeffects typically occur when microbubbles are undergoing inertial cavitation. ICD is a method for determining the overall bubble activity over treatment duration, and was used in this study to relate bubble behavior to AuNP accumulation. As acoustic pressure increased, ICD, measured in arbitrary units, increased. ICD increased the most dramatically from 570 kPa to 770 kPa. This great increase in ICD suggests that between 570 kPa and 770 kPa there is a fundamental change in bubble activity. Demonstrated in a previous study, it has been determined that inertial cavitation threshold for this experimental design is at 620 kPa, showing great increases in bubble activity after that pressure threshold which supports the massive increase at 770 kPa [74]. In inertial cavitation, bubbles collapse generating a high magnitude broadband acoustic signal[61] such as was seen at 770 kPa. Thus, it is reasonable to suggest that the greatest increase in cellular accumulation of AuNP which is observed at 770 kPa is due to the change in bubble behavior to the inertial regime. Moreover, when comparing accumulation with ICD we see a linear trend between cellular accumulation of AuNP of all types. Previous work done by this group has demonstrated that the accumulation of both FITC[70] and cisplatin[75] are proportional to ICD, supporting the results found in this study for AuNP between 10-50 nm. Thus it can be inferred that the increase in accumulation observed in AuNP due to USMB is directly proportional to bubble activity measured by ICD.

4.2 AuNP+USMB+XRT Survival fraction

Radiation therapy of 225 kVp at a dose of 2 Gy, experienced a large improvement to treatment efficacy with the presence of AuNP and USMB at ultrasound conditions of 770 kPa. These acoustic setting were found to be optimal in regards to cellular accumulation of the AuNP and thus were chosen for this part of the study. For all AuNP types used, it was found that the resulting decrease in cell viability from AuNP+USMB+XRT was synergistic when compared to XRT and USMB+AuNP alone. Radiation sensitization and treatment enhancement is proportional to mass of gold as shown by Hainfeld et al. When comparing the survival of mice after radiation treatments, it was found that administering 1.35g/kg of AuNP prior to treatments resulted in an increase in yearlong survival from 20% to 50%. Additionally, when doubling the AuNP concentration, it was found that survival increased to 86%[34]. Furthermore, another in vivo study by Zhang et al, measured tumor volume reduction using AuNP and XRT. Comparing AuNP of different sizes, it was found that 12.1 nm AuNP had optimal delivery into the tumor region compared to larger (targeted by macrophages and accumulated in liver) or smaller (excreted through the kidney) and as a results, achieved tumor volume reduction while the AuNP of other sizes, while better than XRT alone, saw increases in tumor volume[2]. Therefore, it is evident that the synergism we see when combining USMB+AuNP+XRT is likely a result of the approximately 3 fold increase in cellular accumulation of the AuNP observed when treated with USMB at 770 kPa.

Additionally, USMB has been shown to synergistically improve cell death in tumors when combined with XRT by the production of ceramide, which is linked to vascular disruption resulting in reduced tumor volumes when combining USMB+XRT than XRT alone in vivo[66]. In this study performed by Atala et al, cell viability within PC3 tumors was reduced 10 fold when comparing USMB+XRT and XRT alone.

When comparing the survival fraction of 50 nm and 10 nm AuNP, it is evident that the significantly larger cellular accumulation, both with and without USMB, of 50 nm AuNP does not show greater treatment efficacy than the 10 nm AuNP. Comparing the survival fraction of AuNP+XRT of 50

nm and 10 nm, with and without USMB, we observed no statistical difference between the two sizes ($P>0.05$). At first glance this seems counterintuitive since there is 30% and 50% more intercellular gold content for 50 nm AuNP compared to 10 nm with and without USMB respectively. One explanation might be that the larger AuNP experienced more internal absorption of energy during photo electric events. Due to the nature of low ionization energy interactions with gold, several Auger electrons are produced per event which deposit energy in a local region near the AuNP. However, the larger the AuNP, the more likely that the energy is deposited internally, as the Auger electrons need to travel further within the particle to escape. A Monte Carlo study performed by Pignol et al, simulated the energy deposited from single photoelectric events for different sizes of AuNP and radiation energies. As particle size increased, there was more energy per photo electric event that was absorbed internally by the gold, mostly coming in the form of Auger electrons failing to escape. This was especially true at low ionizing energy levels, such as what was used in this study, with more than 50% reduction of the energy from Auger electrons between 100 nm AuNP and 5 nm[39]. Another potential explanation for 50 nm AuNP showing less death than 10 nm could be due to the experimental method. Because the same mass of gold per mL of cell solution was used, as opposed to the same concentration which is typically seen in these types of studies[4], the number of AuNP is drastically different between 50 and 10 nm (approximately 40 and 5000 50 nm and 10 nm AuNP per cell respectively). Since both the accumulation measurements were taken on average, it may have been more probable for cells exposed to 50 nm AuNP to have uneven distributions, as there are far fewer particles available to interact per cell. This could result in some cells with large amounts of AuNP and others with none which ICP would not be able to differentiate. When exposed to XRT, there could be less overall improvement in this scenario, where excess gold within a single cell may not translate to overall cell death across a population.

Comparing survival fraction of XRT treatments between AuNP with and without NLS, we found no statistical differences both in the presence and absence of USMB. This is supported by the statistically indifferent accumulation between both types of particles. However, a noteworthy realization is that

AuNP with NLS appear to reduce survival fraction in conjunction with USMB, but not without. Further work should be done to determine if this trend holds any significance.

Nuclear localizing signals are designed to allow attached molecules to interact with Importin proteins, so they can be carried through nuclear pores[47,48]. Theoretically this would mean that AuNP with this signal would enhance radiation further than without it, as closer proximity to DNA should improve damage[49,50,76]. One Monte Carlo study done by Cai et al, compared the required number of AuNP to double the dose dependent on location for 30 nm AuNP. It was found in all models used (single cell, monolayer and 3D) that it required less AuNP to double the dose at all energies, with a difference of 25 to 100 AuNP for nuclear and cytoplasmic localization respectively, at a 100 keV and a monolayer model[76]. The problem when adding NLS to AuNP is that the method of cellular delivery, endocytosis, leaves the particle within endosomes and unable to interact with the required proteins for nuclear transport. Thus it has been shown that without a method of escaping endosomal entrapment, like an additional peptide, there will be no nuclear targeting[45]. In case of this study no such peptide was added, meaning that on its own, the 10 nm with NLS would not enter the nucleus. Using the Cytoviva hyperspectral camera, it was possible to ascertain the location of AuNP within cells using their unique reflectance from Surface Plasmon Resonance. In the obtained images, it appears that NLS on its own did not allow the AuNP to enter the nucleus, but with USMB it appears that it was possible. The mechanism that potentially caused this to occur might be pore formation. At inertial cavitation regimes, it is possible to generate pores large enough to allow 10 nm AuNP to diffuse through the membrane, without ever becoming entrapped in the endosomal pathway[17]. This would allow the AuNP with NLS to enter cells and interact with the Importin proteins, transporting them into the nucleus, resulting in a reduction in the observed survival fraction supported by Cai et al's Monte Carlo study. Further examination should be considered to better understand if USMB can improve the localization of NLS labeled AuNPs, to determine if this can be used to further benefit XRT.

4.3 Limitations and Future Work

In this study, a cell suspension model was used to allow for passive cavitation detection, but it does not ideally model the adherent properties of the PC3 cell line. Although previous studies have used this design, the result of treating in suspension may alter accumulation results potentially due to different cell endocytosis behaviors when in suspension.

Future work for will include methods to further increase the cellular accumulation of AuNP when exposed to USMB, like the use of an antidepressant known as Desipramine[26]. Additionally, accumulation results will be measured with the use of nanobubbles instead of microbubbles. Lastly, the treatment will be applied to mice in vivo to better understand USMB's effect on the distribution of molecules from vasculature to tumor regions.

5 Conclusion

The combined treatment of PEGylated AuNP, ultrasound stimulated microbubbles and XRT has shown to be synergistic in PC3 prostate cancer cells this study. With a minimum survival fraction of 0.11 for USMB+10 nm AuNP with NLS+XRT compared to 0.56 for XRT alone, we have seen greater than a 5 fold increase in treatment efficacy. The synergistic improvement has been linked to enhanced accumulation caused by the exposure of cells to USMB. By measuring the accumulation of AuNP of 50 nm, 10 nm and 10 nm with NLS with ICP AES, it was discovered that accumulation of AuNP was proportional to peak negative pressure, with a maximum accumulation occurring at 770 kPa. While 50 nm AuNP showing higher magnitudes of intercellular accumulation for all conditions, all 3 types of AuNP increased in relative accumulation by about 3 fold with USMB at optimal acoustic parameters compared to untreated samples. Increasing ultrasound peak negative pressure resulted in increasing bubble activity measured by ICD, with the greatest change to bubble activity occurring past the inertial cavitation threshold. Comparing accumulation to ICD showed a linear relationship, suggesting a direct correlation between bubble activity and accumulation. Additionally, it was shown that although 50 nm AuNP have the highest accumulation, it did not outperform smaller nanoparticles, with comparable

survival fractions. USMB also potentially demonstrated the ability to facilitate nuclear localization, which may explain the apparent reduction in survival fraction of 10 nm with NLS compared to 10 nm for USMB+AuNP+XRT treatments. USMB alone also displayed synergism when combined with XRT, further cementing its viability for use in radiation enhancement strategies. Overall, this study demonstrated the significance of combining USMB with AuNP+XRT by increasing cellular accumulation of 10 and 50 nm AuNP in proportion to bubble activity and by synergistically enhancing XRT.

Bibliography

1. Hainfeld, J. F., Slatkin, D. N. & Smilowitz, H. M. The use of gold nanoparticles to enhance radiotherapy in mice. *Phys. Med. Biol.* **49,** (2004).

2. Zhang, X. D. *et al.* Size-dependent radiosensitization of PEG-coated gold nanoparticles for cancer radiation therapy. *Biomaterials* **33,** 6408–6419 (2012).

3. Chithrani, B. D. & Chan, W. C. W. Elucidating the mechanism of cellular uptake and removal of protein-coated gold nanoparticles of different sizes and shapes. *Nano Lett.* **7,** 1542–1550 (2007).

4. Chithrani, B. D., Ghazani, A. A. & Chan, W. C. W. Determining the size and shape dependence of gold nanoparticle uptake into mammalian cells. *Nano Lett.* **6,** 662–668 (2006).

5. Chithrani, D. B. Intracellular uptake, transport, and processing of gold nanostructures. *Mol. Membr. Biol.* **27,** 299–311 (2010).

6. Wilhelm, S. *et al.* Analysis of nanoparticle delivery to tumours. *Nature Reviews Materials* **1,** (2016).

7. Schuemann, J. *et al.* Roadmap to clinical use of gold nanoparticles for radiation sensitization. *Int. J. Radiat. Oncol. Biol. Phys.* **94,** 189–205 (2016).

8. Karshafian, R., Samac, S., Bevan, P. D. & Burns, P. N. Microbubble mediated sonoporation of cells in suspension: Clonogenic viability and influence of molecular size on uptake. *Ultrasonics* **50,** 691–697 (2010).

9. Zhou, Y. Ultrasound-Mediated Drug/Gene Delivery in Solid Tumor Treatment. *J. Healthc. Eng.* **4,** 223–254 (2013).

10. Liao, A. H. *et al.* Estimating the Delivery Efficiency of Drug-Loaded Microbubbles in Cancer

Cells with Ultrasound and Bioluminescence Imaging. *Ultrasound Med. Biol.* **38,** 1938–1948 (2012).

11. Dimcevski, G. *et al.* A human clinical trial using ultrasound and microbubbles to enhance gemcitabine treatment of inoperable pancreatic cancer. *J. Control. Release* **243,** 172–181 (2016).

12. Lentacker, I., Geers, B., Demeester, J., De Smedt, S. C. & Sanders, N. N. Design and evaluation of doxorubicin-containing microbubbles for ultrasound-triggered doxorubicin delivery: Cytotoxicity and mechanisms involved. *Mol. Ther.* **18,** 101–108 (2010).

13. Micromarker, V. *et al.* Enhanced gene transfection using ultrasound. *Nature* 1586–1589 (2010).

14. Fan, Z., Chen, D. & Deng, C. X. Improving ultrasound gene transfection efficiency by controlling ultrasound excitation of microbubbles. *J. Control. Release* **170,** 401–413 (2013).

15. Ferrara, K., Pollard, R. & Borden, M. Ultrasound Microbubble Contrast Agents: Fundamentals and Application to Gene and Drug Delivery. *Annu. Rev. Biomed. Eng.* **9,** 415–447 (2007).

16. Sirsi, S. R. & Borden, M. A. Advances in ultrasound mediated gene therapy using microbubble contrast agents. *Theranostics* **2,** 1208–1222 (2012).

17. Meijering, B. D. M. *et al.* Ultrasound and microbubble-targeted delivery of macromolecules is regulated by induction of endocytosis and pore formation. *Circ. Res.* **104,** 679–687 (2009).

18. Lentacker, I., De Cock, I., Deckers, R., De Smedt, S. C. & Moonen, C. T. W. Understanding ultrasound induced sonoporation: Definitions and underlying mechanisms. *Adv. Drug Deliv. Rev.* **72,** 49–64 (2014).

19. De Cock, I. *et al.* Ultrasound and microbubble mediated drug delivery: acoustic pressure as determinant for uptake via membrane pores or endocytosis. *J. Control. Release* **197,** 20–28 (2015).

20. Hu, Y., Wan, J. M. F. & Yu, A. C. H. Membrane Perforation and Recovery Dynamics in

Microbubble-Mediated Sonoporation. *Ultrasound Med. Biol.* **39,** 2393–2405 (2013).

21. Zhou, Y., Kumon, R. E., Cui, J. & Deng, C. X. The Size of Sonoporation Pores on the Cell Membrane. *Ultrasound Med. Biol.* **35,** 1756–1760 (2009).

22. Kumon, R. E. *et al.* Spatiotemporal Effects of Sonoporation Measured by Real-Time Calcium Imaging. *Ultrasound Med. Biol.* **35,** 494–506 (2009).

23. Mehier-Humbert, S., Bettinger, T., Yan, F. & Guy, R. H. Plasma membrane poration induced by ultrasound exposure: Implication for drug delivery. *J. Control. Release* **104,** 213–222 (2005).

24. Derieppe, M. *et al.* Recruitment of endocytosis in sonopermeabilization-mediated drug delivery: A real-time study. *Phys. Biol.* **12,** 46010 (2015).

25. Doinikov, A. A. & Bouakaz, A. Theoretical investigation of shear stress generated by a contrast microbubble on the cell membrane as a mechanism for sonoporation. *J. Acoust. Soc. Am.* **128,** 11–19 (2010).

26. Fekri, F., Delos Santos, R. C., Karshafian, R. & Antonescu, C. N. Ultrasound microbubble treatment enhances clathrin-mediated endocytosis and fluid-phase uptake through distinct mechanisms. *PLoS One* **11,** 1–22 (2016).

27. Baskar, R., Lee, K. A., Yeo, R. & Yeoh, K. W. Cancer and radiation therapy: Current advances and future directions. *Int. J. Med. Sci.* **9,** 193–199 (2012).

28. Podgorsak. Radiation physics for Medical Physicists.

29. Korideck, H. Targeted Radiotherapy with gold nanoparticles. **9,** 1063–1082 (2014).

30. He, C. & C.L. Chow, J. Gold nanoparticle DNA damage in radiotherapy: A Monte Carlo study. *AIMS Bioeng.* **3,** 352–361 (2016).

31. Matsudaira, H., Ueno, A. M. & Furono, I. Iodine Contrast Medium Sensitizes Cultured Mammalian Cells to X Rays but Not to γ. **84,** 144–148 (2016).

32. Iwamoto, K. S. *et al.* Radiation dose enhancement therapy with iodine in rabbit VX-2 brain tumors. *Radiother. Oncol.* **8,** 161–170 (1987).

33. Connor, E. E., Mwamuka, J., Gole, A., Murphy, C. J. & Wyatt, M. D. Gold nanoparticles are taken up by human cells but do not cause acute cytotoxicity. *Small* **1,** 325–327 (2005).

34. Hainfeld, J. F., Dilmanian, F. A., Slatkin, D. N. & Smilowitz, H. M. Radiotherapy enhancement with gold nanoparticles. *J. Pharm. Pharmacol.* **60,** 977–985 (2008).

35. Pignol, J. P., Rakovitch, E., Beachey, D. & Le Sech, C. Clinical significance of atomic inner shell ionization (ISI) and Auger cascade for radiosensitization using IUdR, BUdR, platinum salts, or gadolinium porphyrin compounds. *Int. J. Radiat. Oncol. Biol. Phys.* **55,** 1082–1091 (2003).

36. Jain, S. *et al.* Cell-Specific Radiosensitization by gold nanoparticles at megavoltage radiation energies. *Int. J. Radiat. Oncol. Biol. Phys.* **79,** 531–539 (2011).

37. Mesbahi, A., Jamali, F. & Gharehaghaji, N. Effect of photon beam energy, gold nanoparticle size and concentration on the dose enhancement in radiation therapy. *BioImpacts* **3,** 29–35 (2013).

38. McMahon, S. J. *et al.* Nanodosimetric Effects of Gold Nanoparticles in Megavoltage Radiation Therapy. *Radiother. Oncol.* **100,** 412–416 (2011).

39. Pignol, J. P. & Lechtman, E. Implications on clinical scenario of gold nanoparticle radiosensitization in regards to photon energy, nanoparticle size, concentration and location. *Phys. Med. Biol.* **57,** 291–295 (2012).

40. Pan, Y. *et al.* Size-dependent cytotoxicity of gold nanoparticles. *Small* **3,** 1941–1949 (2007).

41. Hossain, M. & Su, M. Nanoparticle location and material-dependent dose enhancement in X-ray

radiation therapy. *J. Phys. Chem. C* **116,** 23047–23052 (2012).

42. Ng, C. T. *et al.* Clathrin-mediated endocytosis of gold nanoparticles in vitro. *Anat. Rec.* **298,** 418–427 (2015).

43. Ding, H. ming & Ma, Y. qiang. Role of physicochemical properties of coating ligands in receptor-mediated endocytosis of nanoparticles. *Biomaterials* **33,** 5798–5802 (2012).

44. Hao, X. *et al.* Caveolae-mediated endocytosis of biocompatible gold nanoparticles in living Hela cells. *J. Phys. Condens. Matter* **24,** (2012).

45. Cruje, C. Enhanced Uptake of Polyethylene Glycol Coated Gold Nanoparticles for. (2015).

46. Pramanik, A. K., Siddikuzzaman, Palanimuthu, D., Somasundaram, K. & Samuelson, A. G. Biotin Decorated Gold Nanoparticles for Targeted Delivery of a Smart-Linked Anticancer Active Copper Complex: In Vitro and in Vivo Studies. *Bioconjug. Chem.* **27,** 2874–2885 (2016).

47. Pemberton, L. F. & Paschal, B. M. Mechanisms of receptor-mediated nuclear import and nuclear export. *Traffic* **6,** 187–198 (2005).

48. Fahrenkrog, B. The nuclear pore complex, nuclear transport, and apoptosisThis paper is one of a selection of papers published in this Special Issue, entitled The Nucleus: A Cell Within A Cell. *Can. J. Physiol. Pharmacol.* **84,** 279–286 (2006).

49. Tkachenko, A. G. *et al.* Multifunctional gold nanoparticle-peptide complexes for nuclear targeting. *J. Am. Chem. Soc.* **125,** 4700–4701 (2003).

50. Yang, C., Uertz, J., Yohan, D. & Chithrani, B. D. Peptide modified gold nanoparticles for improved cellular uptake, nuclear transport, and intracellular retention. *Nanoscale* **6,** 12026–12033 (2014).

51. Englebienne, P., Hoonacker, A. Van & Verhas, M. Surface Plasmon Resonance Principles

Methods Applications. *Spectroscopy* **17,** 255–273 (2003).

52. Huang, X. & El-Sayed, M. A. Gold nanoparticles: Optical properties and implementations in cancer diagnosis and photothermal therapy. *J. Adv. Res.* **1,** 13–28 (2010).

53. Li, S. D. & Huang, L. Stealth nanoparticles: High density but sheddable PEG is a key for tumor targeting. *J. Control. Release* **145,** 178–181 (2010).

54. Jesse V Jokerst, Tatsiana Lobovkina, R. N. Z. and S. S. G. Nanoparticle PEGylation for imaging and therapy. *Nanomedicine* **6,** 715–728 (2012).

55. England, C. G., Gobin, A. M. & Frieboes, H. B. Evaluation of uptake and distribution of gold nanoparticles in solid tumors. *Eur. Phys. J. Plus* **130,** 1–16 (2015).

56. Yohan, D. Darren thesis. (2015).

57. Schuemann, J. *et al.* Roadmap to clinical use of gold nanoparticles for radiation sensitization. *Int. J. Radiat. Oncol. Biol. Phys.* **94,** 189–205 (2016).

58. Dijkmans, P. A. *et al.* Microbubbles and ultrasound: From diagnosis to therapy. *Eur. J. Echocardiogr.* **5,** 245–256 (2004).

59. Hoff, L., Sontum, P. C. & Hovem, J. M. Oscillations of polymeric microbubbles: Effect of the encapsulating shell. *J. Acoust. Soc. Am.* **107,** 2272–2280 (2000).

60. Chomas, J., Dayton, P., Allen, J., Morgan, K. & Ferrara, K. Mechanisms of Contrast Agent Destruction. 232–248 (2001).

61. King, D. A. *et al.* Using passive cavitation detection to observe postexcitation response of ultrasound contrast agents. *Proc. - IEEE Ultrason. Symp.* 1286–1289 (2009). doi:10.1109/ULTSYM.2009.5441685

62. Santin, M. D. *et al.* Encapsulated Contrast Microbubble Radial Oscilation Associated with Postexitation Pressure Peaks. *J. Acoust. Soc. Am.* **127,** 1156–1164 (2010).

63. Bull, J. L. The application of microbubbles for targeted drug delivery. *Expert Opin. Drug Deliv.* **4,** 475–493 (2007).

64. Karshafian, R. & Burns, P. N. Ultrasound and microbubble mediated generation of transient pores on cell membranes in vitro. *Proc. - IEEE Ultrason. Symp.* 1805–1808 (2009). doi:10.1109/ULTSYM.2009.5441643

65. Lammertink, B., Deckers, R., Storm, G., Moonen, C. & Bos, C. Duration of ultrasound-mediated enhanced plasma membrane permeability. *Int. J. Pharm.* **482,** 92–98 (2015).

66. Atala, A. Re: Tumor radiation response enhancement by acoustical stimulation of the vasculature. *J. Urol.* **189,** 1163 (2013).

67. Kim, H. C., Al-Mahrouki, A., Gorjizadeh, A., Karshafian, R. & Czarnota, G. J. Effects of biophysical parameters in enhancing radiation responses of prostate tumors with ultrasound-stimulated microbubbles. *Ultrasound Med. Biol.* **39,** 1376–1387 (2013).

68. Rotolo, J. *et al.* Anti-ceramide antibody prevents the radiation gastrointestinal syndrome in mice. *J. Clin. Invest.* **122,** 1786–1790 (2012).

69. Al-Mahrouki, A. A., Karshafian, R., Giles, A. & Czarnota, G. J. Bioeffects of Ultrasound-Stimulated Microbubbles on Endothelial Cells: Gene Expression Changes Associated with Radiation Enhancement In Vitro. *Ultrasound Med. Biol.* **38,** 1958–1969 (2012).

70. Kudo, N., Okada, K. & Yamamoto, K. Sonoporation by single-shot pulsed ultrasound with microbubbles adjacent to cells. *Biophys. J.* **96,** 4866–4876 (2009).

71. Honda, H., Kondo, T., Zhao, Q. L., Feril, L. B. & Kitagawa, H. Role of intracellular calcium ions

and reactive oxygen species in apoptosis induced by ultrasound. *Ultrasound Med. Biol.* **30,** 683–692 (2004).

72. Escoffre, J. M., Piron, J., Novell, A. & Bouakaz, A. Doxorubicin delivery into tumor cells with ultrasound and microbubbles. *Mol. Pharm.* **8,** 799–806 (2011).

73. Juffermans, L. J. M., Kamp, O., Dijkmans, P. A., Visser, C. A. & Musters, R. J. P. Low-Intensity Ultrasound-Exposed Microbubbles Provoke Local Hyperpolarization of the Cell Membrane Via Activation of BKCa Channels. *Ultrasound Med. Biol.* **34,** 502–508 (2008).

74. Momin, S. On the Acoustic Response of Ultrasonically - Stimulated microbbubbles and Enhance Intracellular Uptake of a Fluorescent Molecule. (2016).

75. Sheliza, J. Synergistic Cisplatin-Induced Cell Death By Ultrasound-Microbubble Mediated Intracellular Delivery in Breast Cancer Cells (2016).

76. Cai, Z. *et al.* Investigation of the effects of cell model and subcellular location of gnp. *Med. Phys. Med. Phys* **40,** (2013).

77. Kang, B., Mackey, M. A. & El-Sayed, M. A. Nuclear targeting of gold nanoparticles in cancer cells induces DNA damage, causing cytokinesis arrest and apoptosis. *J. Am. Chem. Soc.* **132,** 1517–1519 (2010).